Lund University

Master Thesis

Dosimetric investigations of dynamic effects during Immunostimulating Interstitial Laser Thermotherapy

Author:

Hampus Mårtensson Jönsson

Supervisors:

Prof. Lars Engström,

Dr. Johan Axelsson

& Cristina Pantaleone

A thesis submitted in fulfilment of the requirements for the degree of Master of Science

in the

Division of Atomic Physics

Department of Physics

June 2017

Lund University

Faculty of Science

LUND UNIVERSITY

Abstract

Faculty of Science
Department of Physics

Master of Science

Dosimetric investigations of dynamic effects during Immunostimulating Interstitial Laser Thermotherapy

by Hampus Mårtensson Jönsson

A simulation model of immunostimulating Interstitial Laser Thermotherapy (imILT) has been developed to investigate the effect that biological variations in tissues have on the treatment outcome. The biological variations include optical and thermal properties. The model based on the results of these investigations was further developed to investigate the possibility of predicting an imILT treatment outcome on *ex vivo* bovine cardiac muscle tissue, and experiments were performed to validate the simulations. An imILT treatment is based on laser induced tissue ablation due to heat generation via light absorption. The optical properties, i.e. the absorption and the reduced scattering coefficient, affect the treatment outcome in a similar way. An increase in these coefficients yields a faster temperature rise closer to the light source. Furthermore it was seen that it is important to take into consideration a change in optical properties related to thermal coagulation of tissue since the optical properties of coagulated tissue are significantly different from non-coagulated tissue of the same type due to the increased scattering. The effect of varying the thermal properties on the treatment outcome was found to be governed by heat conductivity. Changes in the model were thus made to account for the effects due to tissue coagulation and the heat conductivity by implementing a dynamic relationship between temperature and the optical and thermal properties. The simulated results were found to be in good qualitative agreement with the experiments.

Acknowledgements

I would like to thank my supervisors Cristina Pantaleone, Dr. Johan Axelsson, and Professor Lars Engström, who have in every possible way helped me throughout this project. Thank you for your commitment and your positivity. I would also like thank my temporary co-workers at CLS for the enjoyable work environment they provided. Furthermore, I would like to thank Emily Emilsson with whom I collaborated with in regard to the parts of the experimental work that was performed during the duration of her thesis.

Contents

Abbreviations

LITT	**L**aser-**i**nduced **T**hermo**t**herapy
CLS	**C**linical **L**aserthermia **S**ystems
imILT	**im**munostimulating **I**nterstitial **L**aser **T**hermotherapy
Nd:YAG	**n**eodymium-**d**oped **y**ttrium **a**luminium **g**arnet
MFP'	Transport **M**ean **F**ree **P**ath
FEM	**F**inite **E**lement **M**ethod
PBS	**P**hosphate-**b**uffered **S**aline

Symbols

g	anisotropy factor	
c_p	specific heat capacity	J/(kg·K)
k	heat conductivity	W/(m·K)
ρ	density	kg/m^3
μ_a	absorption coefficient	cm^{-1}
μ_s	scattering coefficient	cm^{-1}
μ'_s	reduced scattering coefficient	cm^{-1}

Chapter 1

Introduction

Laser light has been used for a wide variety of applications, and within the medical field it was already employed in the early 1980's. It was for example introduced in the form of laser-induced interstitial thermotherapy (LITT) by e.g. Bown in 1983 [1]. Laser-induced interstitial thermotherapy can be used as a mean of minimally invasive tumour ablation, and has an advantage over traditional surgical methods regarding for example treatment of primary and metastatic focal malignancy, tumours in poor operative candidates, and pain palliation [2] because of its less invasive treatment approach. Another advantage with using laser light for thermal therapy is that it can deposit a precise amount of energy in a well-defined region, which in turn induces lesions (accumulated tissue damage) of reproducible size [3].

The technique which this thesis is focused on is called Immunostimulating Interstitial Laser Thermotherapy (imILT^{CLS}), and has been developed by Clinical Laserthermia Systems (CLS), based in Lund, Sweden [4]. imILT is based on LITT, and is a treatment technique developed to treat cancerous tissue. In addition to eradicating the primary tumour, imILT has been shown to induce a potential release of tumour specific antigens resulting in a systematic immune activation against

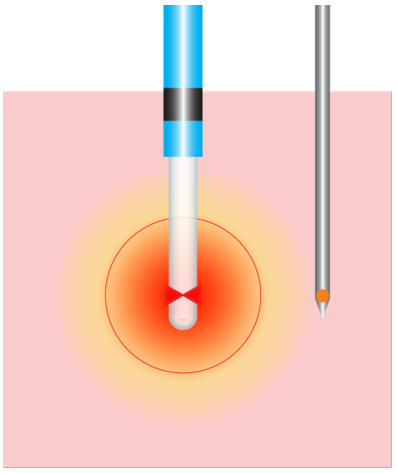

FIGURE 1.1: A sketch of an ImILT treatment, where an optical fiber (thicker) acts as a light and heat source, and a temperature probe (thinner) acts as a temperature feedback sensor.

remaining cancer cells in the treated region [5].

An immunostimulating interstitial laser thermotherapy treatment session is initiated by delivering laser light via an optical fiber to the tissue of interest, which induces a temperatue gradient within the tissue (figure 1.1). The clinical practice is thereafter to increase the temperature at the tumour border to 46° C and to maintain this temperature for 30 minutes, considered the treatment time. The reason for having a treatment time of 30 minutes at this low target-temperature is to ensure complete cell necrosis in the targeted tissue [6], and induce an immunologically driven anti-tumour response [7].

Regarding the application of imILT, an expanded understanding of light-tissue interaction and the subsequent heating of tissue is of importance, since it governs the thermally induced effects the tissue experiences. Two tissues of the same type do not have the same optical and thermal properties due to variations in for example blood content, water content, and fiber development, and thus implies that a specific tumour type has varied properties between different patients. Thus, it is of importance to understand how a difference in these properties for the same tissue type can effect the outcome of a treatment, and how large of an error this yields for a certain protocol. Furthermore, it is also known that the different properties of tissue can dynamically change during a laser-based thermotherapy treatment, which means that a static model yields a possibly large inaccuracy [8]. A greater knowledge of these effects during treatment can be used to investigate the possibility of predicting the outcome of a *in vivo* imILT treatment.

Aim of the thesis

The aim of this thesis is to develop a simulation model of imILT to investigate:

- the effect on the treatment outcome when:
  - introducing a variation in thermal and optical properties
  - inducing changes in these properties based on conditions such as thermal tissue coagulation

- the possibility of predicting a treatment outcome by using the previous simulation results to develop a dynamic model regarding thermally induced effects in tissue

This will be performed in one part by conducting *ex vivo* imILT experiments on bovine cardiac muscle tissue (using a protocol used in [5], developed by CLS), and in one part by recursively developing a simulation model based on the results and evaluations of the experiments and previous simulations in a iterative manner, beginning with varying optical and thermal properties close to reference data of bovine cardiac muscle tissue. Note that a similar tissue model was simultaneously developed in [9] regarding fixed parameters for bovine cardiac muscle tissue. These two models were however developed independently of each other, and the aim in [9] was to investigate the thermal effect on different components in optical fibers.

Chapter 2

Light-tissue interaction

2.1 Tissue Optics

To better understand how light interacts with tissue, the physiology, biochemistry, and morphology of tissue needs to be translated into optical parameters that will represent a tissue average in regard to its interaction with light. This section will focus on scattering and absorption which are the two fundamental optical properties in tissue. These two processes are then used to describe light transport in tissue via the diffusion theory.

2.1.1 Optical properties of tissue

Consider a beam of light delivered into a medium via an optical fiber. The light mainly interacts with the particles within the medium via absorption and scattering, and in what amount defines the optical properties of the medium. Regarding the interplay between light and particles, scattering and absorption have two different roles. Absorption is considered to transfer all of the photon energy to the absorbing particle, whilst scattering can occur in two ways. These are inelastic scattering and elastic scattering. There exists several inelastic scattering phenomena, but these processes are typically much weaker than elastic scattering [10] and may thus be ignored in this thesis. Regarding elastic scattering such as Mie scattering and Rayleigh scattering, the energy is conserved in the scattering process. Mie scattering occurs when the wavelength is comparable to or smaller than the the particle size, and Rayleigh scattering occurs for wavelength larger than

the particle size [11]. The components of biological tissue in regard to a theoretical analysis of scattering, are assumed to be spherically shaped particles, and the electromagnetic wave propagation is then modelled via Mie theory. Here, the scattering from one sphere can be described by the radiation caused by a dipole induced through the interaction with the incident electromagnetic field [12].

The majority of biological tissues are considered to be *scattering media* or *turbid media* due to their strong optical scattering characteristics in the visible to the near infrared wavelength range [13]. The whitish colour of tissue, rather than black, demonstrates that tissue scatters visible light. Optical scattering of light in tissue occurs due to for example random spatial variations in the refractive index, and in tissue density, where these properties are related to the heterogeneity of tissue. The absorption of light in tissue is in contrast to scattering mainly governed by the concentration of tissue components that absorb light, so called *Chromophores*. Important chromophores in the visible wavelength range are oxyhemoglobin, deoxyhemoglobin (oxygenated blood and deoxygenated blood respectively), and melanin (pigment granules in the skin and eye), while water is an important chromophore for light of infrared wavelengths [14]

Biological tissue can however be optically characterized by having small and uniformly distributed scattering and absorption centres throughout the tissue, and these can in turn be characterized by the scattering coefficient, μ_s (mm^{-1}), and the absorption coefficient, μ_a (mm^{-1}), respectively. These coefficients represent the inverse of the mean free path between scattering events and until absorption, respectively [13]. Another component regarding scattering in biological tissue is the anisotropy factor, g, given by

$$\langle \cos\theta \rangle = g \tag{2.1}$$

which is defined as the mean cosine of the scattering angle of light (θ) and thus describes the angular distributon of light in the tissue. The value of the anisotropy factor can vary between -1 and 1 where the g-values of -1, 0 and 1 represent complete backward, isotropic and complete forward scattering of light respectively [14]. A typical value of g for tissue in the visible and near-infrared region is larger than 0.9, implying the forward-scattering nature of tissue [3]. Combining the anisotropy factor and the scattering coefficient, the reduced scattering coefficient,

μ_s', can be introduced [13]:

$$\mu_s' = (1 - g)\mu_s \tag{2.2}$$

The spectral region between 600-1300 nm is often refered to as the tissue optical window, this being possible mainly due to a lack of strong absorption by blood. The tissue optical window is thus of interest for biomedical optics since a much longer penetration depth can be achieved here [15]. Photons in this wavelength range propagating in biological tissue has an average mean path length between two scattering events of about 0.1 mm, and a mean absorption length of about 10-100 mm [16]. For this reason, lasers emitting light with a wavelength of 1064 nm, such as the Nd:YAG Laser, can be utilized. This is because a deeper penetration of the light into the tissue allows for a higher power deposition, which in turn allows for a larger volume of possible necrosis.

2.1.2 Light transport - Diffusion theory

How light is distributed throughout a medium can be described by treating it as a concentration of optical energy that diffuses down a concentration gradient. This description of light used when simulating light transport using the diffusion theory assumes that the quantity diffusing, in this case optical energy, does not have a preferred direction of travel. Thus, the net movement of that quantity is by diffusion down a concentration gradient, following Fick's first law of diffusion [17].

A collimated beam of light entering tissue from an optical fiber has a defined direction of travel. However, due to the highly scattering nature of biological tissue, the incoming photons quickly loose their directionality (due to multiple scattering events) in a distance of $1/[\mu_a + \mu_s']$, called the transport mean free path (or MFP'), which for tissue in the visible or near-infrared region corresponds to 1-2 mm. The MFP' defines the distance from the light source where the diffusion theory is valid, and can be said to be the point of origin for the diffusion process. Another assumption made by the diffusion theory of light is that photons are able to participate in random walk, meaning that the photons should undergo many scattering events before being absorbed. A commonly cited rule of thumb is that the ratio μ_s'/μ_a should be larger than 10 for the diffusion theory to be valid.

A mathematical description of the diffusion theory of light in a form designed for numerical analysis, in this case, a partial differential equation, is given by [17]

$$\overbrace{\frac{1}{c}\frac{\partial\phi(r,t)}{\partial t}}^{\substack{\text{change in}\\ \text{fluence rate}}} - \overbrace{\nabla\cdot D\nabla\phi(\mathbf{r},t)}^{\text{diffused light}} + \overbrace{\mu_a\phi(\mathbf{r},t)}^{\text{absorbed light}} = \overbrace{S(\mathbf{r},t)}^{\text{source term}} \tag{2.3}$$

where the terms seen on the left-hand side represents a loss of photons due to diffusion and absorption, and the right-hand side describes the source term (light source, i.e. gain of photons) $S(\mathbf{r},\mathbf{t})$. Here:

- c (m/s) represents the speed of light in the medium of interest
- ϕ (W/cm^2) is the photon fluence rate and can be regarded as a measure of concentration, where $\phi/c = C$ is the concentration of optical energy
- D (m) is the diffusion coefficient
- μ_a (m^{-1}) is the absorption coefficient

The diffusion coefficient, D, is in this case given by:

$$D = \frac{1}{3(\mu_a + \mu_s')} \tag{2.4}$$

A stationary form of the diffusion theory of light will however be used in this thesis since the light source used represents a continuous-wave laser instead of a pulsed laser. This implies that the light distribution in the medium of interest can be seen as continuous and independent of time, if under the assumption that when the laser is turned on a specific light distribution is generated. Eq. (2.3) thus becomes:

$$-\nabla\cdot D\nabla\phi(\mathbf{r}) + \mu_a\phi(\mathbf{r}) = S(\mathbf{r}) \tag{2.5}$$

An approach to numerically solve a partial diferential equation such as eq. (2.5) for a system of complex boundaries and differing parameters is to utilize the finite element method (FEM), which was used in this thesis. The finite element method is based on solving a partial differential equation for a domain by dividing it into discrete arbitrary elementes with associated equations, which are solved for and thereafter assembled into a larger system. The solution for the problem in the

enitire domain can therafter be calculated using this generated system of sulutions [17].

2.2 Interstitial heat transfer & effects on tissue

Absorbed laser light that is irradiated into biological tissue leads to heat generation and thus to a local temperature rise. How this translates into the resulting heat distribution and injury in biological tissue will be discussed in this section.

2.2.1 Bioheat equation

A way to describe heat generation in biological tissue by absorption of light and the subsequent heat distribution is by utilizing the bioheat-transfer equation, called Pennes' equation [18],[19]:

$$\rho c_p \frac{\partial T}{\partial t} + \nabla(-k\nabla T) = \rho_b c_b \omega_b (T_b - T) + Q_{met} + Q_{ext} \tag{2.6}$$

where:

- ρ and ρ_b (kg/m^3) are the density of tissue and blood respectively
- c_p and c_b (J/(kg·K)) are the specific heat of tissue and blood respectively
- k (W/(m·K)) is the tissue heat conductivity
- T (K) is the local tissue temperature
- ω_b (s^{-1}) is the blood perfusion rate
- T_b (K) is the temperature of arterial blood
- Q_{met} (W/m^3) is the metabolic heat source i.e. heat generated by cell metabolism
- Q_{ext} (W/m^3) is the heat source coupled to light absorption

This equation differs from the classic heat transfer equation by including terms representing cell metabolism and blood perfusion. The classic heat equation describes the distribution of heat in a given region over time due to conduction, and is derived form Fourier's law and conservation of energy. According to Fourier's

law, the rate of flow of thermal energy per unit area through a surface is proportional to the negative of the temperature gradient across the surface, meaning that heat transfer is in the direction of decreasing temperature. In this thesis regarding Pennes' equation Q_{ext} corresponds to heat generation by absorption of laser light, $\mu_a\phi(\mathbf{r})$. The experiments in this thesis were conducted *ex vivo*, and therefore, the blood perfusion rate (ω_b) and the metabolic heat source (Q_{met}) were assumed to be negligible during the simulations performed throughout this thesis work [18].

2.2.2 Laser induced interstitial thermotherapy

The goal of thermotherapy is to destroy tumourous, unhealthy tissue by means of introducing a potent temperature gradient that can kill and disrupt cells in the tumour. At temperatures above 50°C thermal coagulation occurs [3],[20], a form of tissue destruction, which is defined as the thermally induced, irreversible alterations of cellular proteins and other biological molecules. Thermal coagulation can be seen directly after a treatment where it is indicated by a visible whitening of the tissue [21]. The central parts of the coagulated region (necrotic core) is completely denatured and therefore lacking degradative enzymes. The necrotic core is also isolated from the inflammatory cells of the body due to the destruction of blood cells induced by the thermal coagulation [22]. At the temperatures reached during thermal coagulation, the destruction of tumour and normal tissue occurs at the same high rate which implies the importance of applying heat at the precisely right location. An increase of the tissue temperature to above 100°C results in the boiling of water residing in the tissue which leads to steam bubble formation, where these bubbles can coalesce, forming holes in the tissue (illustrated in figure 2.1). Increasing the temperature of dehydrated tissue furthermore, to about 400°C, will initiate tissue burning, resulting in the production of charred tissue and smoke, i.e. carbonization [23].

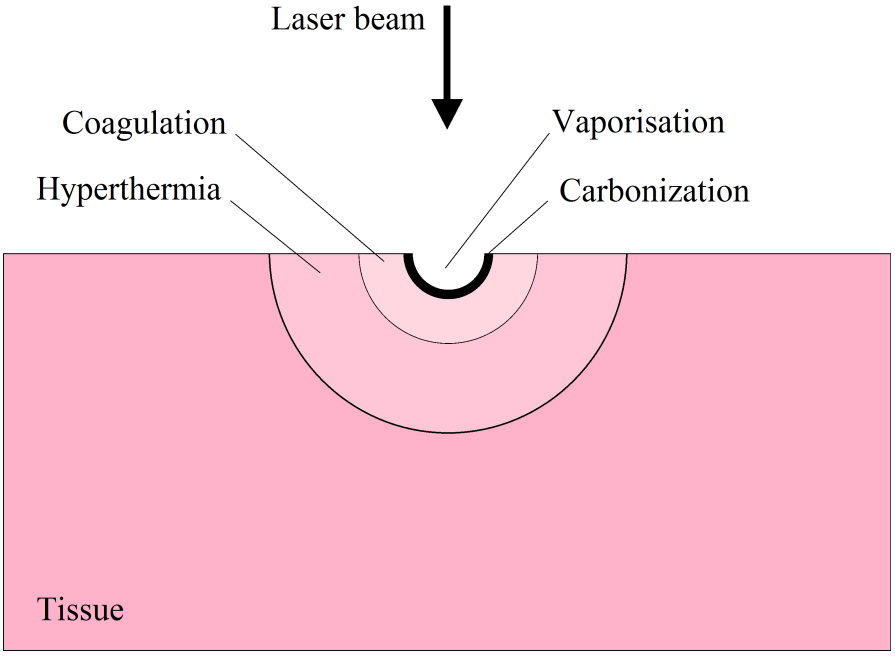

FIGURE 2.1: An illustration of possible thermal effects in biological tissue that can occur during laser induced interstitial thermotherapy. Modified from [18].

Significant thermal effects in tissue due to laser ablation occur for higher power densities such as 10 W/cm^2 from either continuous wave radiation or pulse durations longer than about 1 μs [18]. Typical lasers used for thermotherapy are for example Nd:Yag (neodymium-doped yttrium aluminium garnet) lasers and diode lasers as used in this thesis (continuous wave). Regarding vaporisation and precise thermal cutting, CO_2 lasers are useful [18]. Figure 2.1 shows an example of the thermal effects that can occur during a laser induced interstitial thermotherapy treatment. There are several thermal processes that can occur, where the location and spatial extent of each thermal process depend on the locally achieved temperature during and after laser exposure.

For a quantative approximation of the accumulated thermal damage to biological tissue over a period of time at a certain temperature level, Arrhenius equation, a first-order thermal-chemical rate equation, is useful [18]:

$$\ln \frac{C(t)}{C_0} = -A \int_0^t \exp\left(-\frac{\Delta E_a}{RT(t')}\right) \, dt' = -\Omega(r,t) \tag{2.7}$$

where:

- C_0 is the initial concentration of molecules (or cells), and $C(t)$ is the concentration at a time t
- Ω is the rate constant, and is a dimensionless factor that also can define irreversible thermal injury
- A (s^{-1}) is the frequency factor, and contains information about the frequency and orientation of collisions
- ΔE_a (J/mol) is the activation energy, which defines the energy required for a reaction to occur
- R (J/mol·K) is the universal gas constant of 8.314
- t (s) is the time of heat exposure

The Arrhenius equation can be used to characterize the rate of denaturation of molecules by inserting values for the parameters A and ΔE_a in regard to experimental data for the tissue of interest. The damage integral in eq. (2.7) determines the local degree of tissue damage, and the damge degree is defined as the fraction of deactivated molecules or cells, f_d, [18]:

$$f_d(t) = \frac{C_0 - C(t)}{C_0} = 1 - \exp(-\Omega(t)) \tag{2.8}$$

Experimental research has coupled Ω to the probability of cell death in biological tissue, where $\Omega = 1$ represents a 63% probability of cell death, and $\Omega = 4.6\%$ represents a 99% probability of cell death [34]. The changes in the tissue of interest induced by thermotherapy implies an effect on its optical properties where prominent changes occur during the process of coagulation. It has been shown that coagulated tissue has a larger scattering coefficient than its non-coagulated counterpart, but the difference in the absorption coefficient is nearly negligible [18].

2.2.2.1 Hyperthermia

At the periphery of laser induced interstitial thermotherapy (LITT), the temperature of the treated tissue is lower and no measurable efects in the tissue of interest are observed below 42°C. Heating tissue to temperatures between 42 and 50°C leads to tissue damage on the cellular level, this as a consequence of a number

of different possible processes summarized in the term *hyperthermia*, and is illustrated in figure 2.1 [18]. Structural changes in protein can be induced by heat as a result of breaking hydrogen bonds and disturbing ionic interactions within the macromolecules [24]. Hyperthermia has been shown to remove proteins needed to stabilize the different cell membranes, for which there exists a good correlation to cell death [25]. Another effect that occurs during hyperthermic treatment is the sudden inhibition of the synthesis of cellular DNA, RNA, and proteins [26], for which there has been shown to exist a correspondence to the degree of heating [27]. The cytoskeleton is also affected by hyperthermia, which leads to alterations in the organisation of its various components [28].

The end effects of the thermally induced injuries described above depend on the thermal dose: they are either reversible or lead to tissue death by necrosis or apoptosis (programmed cell death). The term Necrosis is defined as the active degradation process that develops after the death of cells and tissues [3]. The degree of cell death is to some extent increased through apoptosis, which is the cell death mechanism responsible for the physiological elimination of cells [29]. The full extent of cell death can however not be fully analysed with certainty until 24-72 hours after an hyperthermic treatment due to the slow process of the apoptosis (necrosis occurs almost immediatly) [21],[30].

2.3 imILT

Immunostimulating interstitial thermotherapy, formally imILT^{CLS}, a treatment method developed by Clinical Laserthermia Systems (CLS) [4], based on laser induced interstitial thermotherapy (LITT), makes use of thermotherapy at temperatures above and under the requirement for thermal coagulation to treat cancerous tissue. The principle of the procedure is to introduce a temperature gradient in the cancerous tissue of interest by delivering laser light guided by an optical fiber into the tissue; the tumor is heated untill the periphery of the tumor reaches 46°C, and is thereafter kept at this temperature for about 30 minutes. This is performed by adjusting the output power of the laser by turning it off when the temperature at the tumour border is above 46°C and off when lower than 46°C. The 30 minutes treatment time is required since irreversible cell damage at 46°C only occurs after about 30 minutes [6], [31]. In addition to eradicating the primary

tumour, a favourable immunological response, followed by anti-tumour immunity, can be induced by laser thermotherapy [7], [32]. This immunological response can contribute to the destruction of the remaining tumour cells in the treated region, as well as tumour metastasis outside the treatment region.

Chapter 3

Simulations & Experiments

3.1 *Ex vivo* investigation of imILT

In short, the aim of this thesis is to develop a simulation model to analyse how the thermal and optical properties of biological tissue affect the outcome of an imILT treatment. An experimental investigation of imILT was therefore conducted *ex vivo* on bovine cardiac muscle tissue as a reference for validation of the simulation model.

3.1.1 *Ex vivo* experimental set-up

An example of the experimental set-up used in this thesis is shown in figure 3.1. This experimental set-up and the accompanying protocol was developed by CLS [5].

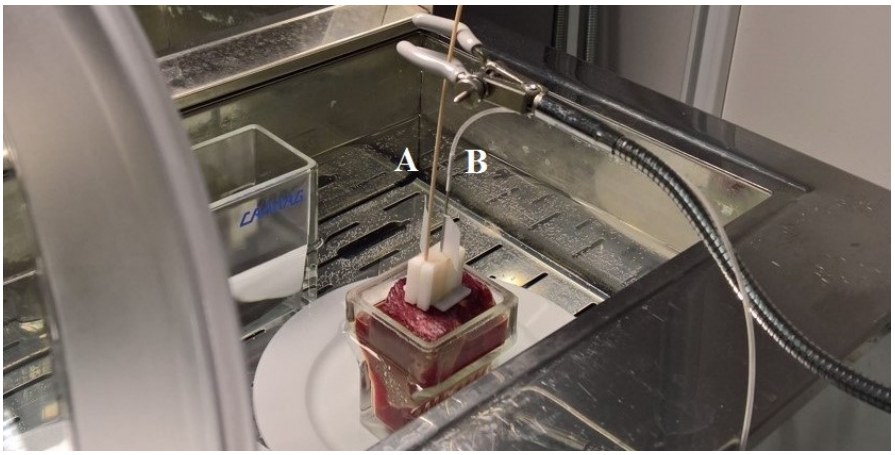

FIGURE 3.1: An example of the *ex vivo* experimental set-up used for an immunostimulating interstitial laser thermotherapy treatment of bovine cardiac muscle. An optical fiber (A) and a temperature measurement probe (B) are inserted into the tissue via a plastic template.

3.1.1.1 Light source

The light source used is a continuous-wave diode-laser with an output wavelength of 1064 nm, and is a part of a laser system tailored to imiLT, named TRANBERG^{CLS} | Mobile Laser Unit, developed by CLS [4]. The unit includes an automatic temperature feedback system that adjusts the output power based on the temperature measured in the tissue of interest.

3.1.1.2 Means of light delivery

A multi-mode *radial fiber* developed by CLS was used to guide the laser-light to the part of the tissue to be heated. This fiber emits the light with a radial (ring-like) intensity profile in a plane perpendicular to the fiber axis, having a divergence angle of approximately 15°. The outer diameter of the fiber is 1.81 mm, and the plane of light emission is located 2 mm above the fiber tip.

3.1.1.3 Temperature measurement probes

Three different temperature measurement probes, single probe 1 (SP1), SP2, and multi probe (MP), developed by CLS were used to monitor the temperature in the treated tissue. SP1 and SP2 measure the temperature using a thermistor located 3 mm above the tip of the probe, and have an accuracy of 0.2°C in the interval between 30 and 70°C. The MP only differs from SP1 and SP2 in that it has in

total four thermistors (MP1, MP2, MP3, MP4) equidistantly spaced by 5 mm along the length of the probe. The temperature sensor used for modulating the laser, *master probe*, can be chosen by the user. The master probe should ideally measure a constant temperature of 46°C during the imILT treatment.

3.1.1.4 Tissue model

The tissue model used for the experiments throughout this thesis work, consists of samples of bovine cardicac muscle tissue cut into even slabs, placed into glass cups containing a PBS (Phosphate-Buffered Saline) solution. These cups are furthermore placed into into a water bath (seen in figure 3.1) where they were heated to the average human body temperature of 37°C and were kept at this temperature during treatment. The PBS solution utilized was used to balance the amount of salt ions in the cells of the tissue, preventing them to burst, and also to prevent the tissue to dry out. Additionally, the PBS solution provides an environment closer to that of the human body. The reason for using a tissue model with bovine cardiac muscle tissue for the experiments in this thesis is because the results can be reproducible [5].

3.1.2 Experimental procedure

The basis of the *ex vivo* experimental procedure for all experiments made in this thesis work was made in the following way: when the temperature of the tissue slab reached 37°C, the fiber and the master probe were inserted parallel to each other at a relative distance of 10 mm with the aid of a plastic template put on top of the slab, as shown in figure 3.1. The template consisted of a solid peace of hard plastic with a set of parallel drilled holes with a 5 mm spacing. The depth of placement into the tissue for the radial fiber and the master probe was 28 mm and 29 mm respectively, thus measuring the temperature at the plane of light emission. The laser's output power was set to 8 W. Note that the output power of the laser increases from 0 W to 8 W in steps of 1 W per second.

At the beginning of the immunostimulating interstitial thermotherapy session, there is a so called *warm-up time*, which is the time required for the laser to heat the tissue to 46°C at the position of the master probe. After the warm-up time the 30 minutes treatment thereafter commenced. After the treatment the tissue slab

was cut along the plane defined by the optical fiber and the master probe. The accumulated damage seen, in this case the visible lesion due to tissue coagulation, was measured using a ruler.

Additionally, a set of *ex vivo* experiments using the same set-up as above plus using all three temperature measurements probes (SP1, SP2, and MP) simultaneously was made. These experiments were performed to see how the temperature changes at points closer and further away from the radial fiber in regard to the master probe, and how these readings compare to the results of the simulation model. The temperature probes that were not acting as the master probe were inserted into the tissue through the plastic template at distances of 5 and 15 mm respectively away from the radial fiber. SP1 and SP2 were placed at a depth of 29 mm, whereas the tip of the MP was placed at a depth of 39 mm, having MP3 in the plane of light emission. Since the MP can measure the temperature at four different depths simultaneously, its position was interchanged with SP1 and SP2 between the treatments.

3.2 Simulating imILT

The imILT simulation model generated in this thesis work was built using the Finite element method oriented software, COMSOL Multiphysics [33]. This software has built-in features for constructing a tissue geometry, as well as for solving the stationary Diffusion (eq. (2.5)) and the Bioheat equation (eq. (2.6)). The light propagation in tissue in the model is given by the diffusion equation which determines where the light propagates. A part of the light is absorbed which leads to the generation of heat. The propagation of the generated heat is determined by the bioheat equation. These equations ((2.5),(2.6)) were solved for in a serial manner in regard to each other, beginning with (2.5). Heat can also induce changes in the optical and thermal properties of tissue which therefore leads to recursive parameters. In this case the parameters for equations equations (2.5) and (2.6) were updated for every time step.

3.2.1 Tissue geometry

Using COMSOL Multiphysics, a square-shaped slab of dimensions $40 \times 40 \times 40$ mm was created as a basis for the tissue geometry. To this slab, the following thermal and optical properties can be allocated in the model:

- ρ (density) $\left[\text{kg m}^{-3}\right]$
- c_p (specific heat) $\left[\text{J kg}^{-1}\ \text{K}^{-1}\right]$
- k (heat conductivity) $\left[\text{W m}^{-1}\ \text{K}^{-1}\right]$
- μ_a (absorption coefficient) $[\text{cm}^{-1}]$
- μ_s' (reduced scattering coefficient) $[\text{cm}^{-1}]$

3.2.2 Modelling Light transport

The stationary form of the diffusion theory (eq. (2.5)), formulated via a stationary Helmholtz equation, was used to simulate light transport in tissue. A point source added at the center of the tissue slab was used as an external light source, representing $S(\mathbf{r})$ in eq. (2.5), and thus the light delivered by the fiber. The optical parameters, μ_a and μ_s' were chosen to correspond to their values for 1064 nm in regard to the tissue of interest. The power allocated to the point source was set to mimic the behaviour of the output power of the laser from the experiments. The power of the light source in the model therefore increases from 0 W to 8 W with steps of 1 W per second. After the warm-up time, the power allocated to the light source when on was approximated to 3 W to approximate the ramp-up behaviour and decrease the computation time. This value was chosen based on the *ex vivo* experiments performed in this thesis.

3.2.3 Modelling heat generation and heat transport in tissue

The bioheat-transfer equation (eq. (2.6)) was used to simulate both heat generation and heat transport in the tissue model. Here, both ω_b and Q_{met} were set to zero. The external heat source, Q_{ext}, was for every point in the model calculated using the simulated light intensity distribution, $\phi(\mathbf{r})$, multiplied by the absorption

coefficient, μ_a. A virtual temperature measurement probe was created to represent the master probe from the experiments and was used to measure the temperature 10 mm away from the light source, and to control the power modulation.

3.2.4 Assessment of tissue damage

The heat-induced damage in the tissue of interest during the imILT simulations was evaluated using two methods to be compared with the experimental results obtained in this thesis. The first method utilizes a temperature threshold at 55°C in regard to thermal coagulation to assess the damaged region of the tissue slab. This temperature threshold was chosen because it is within the defined temperature region for thermal coagulation. The second method is where the Arrhenius equation, eq. (2.7), is used where $\Omega = 4.6$ indicates that 99% of the tissue experiences irreversible thermal damage [34]. These two assessment methods can then be compared to the experimental results, where tissue coagulation is the most visible effect seen directly after a treatment. Regarding the last simulation study a threshold temperature of 60°C was also used to determine tissue coagulation, this to investigate if it gives a resulting lesion closer to the experimentally measured. $\Omega = 1$ corresponding to a 63% probability of cell death [34] was also used in the last simulation study to investigate the possibility of predicting *in vivo* lesion sizes.

3.2.5 Simulation studies

TABLE 3.1: The layout of the different simulation studies performed in this thesis work, including the parameter ranges chosen, and a short description of the corresponding relevance of each study.

Simulation study	**Parameter range**	**Motivation for the study**
Changing the optical properties of tissue	$\mu_a = 0.2$ - 0.4 cm^{-1} and $\mu_s' = 2.96$ - 15.4 cm^{-1}	To investigate the effects of a change in optical properties on the outcome of an imILT treatment
Changing the thermal properties of tissue	$k = 0.197$ - 0.532 W/(m·K) $\rho = 993$ - 1039 kg/m^3 $C_p = 3370$ - 3810 J/kg·K	Same as above in regard to thermal properties
Static coagulation volumes	Volume sizes chosen to be comparable with the experimental results: diameters of 5 - 17 mm	To assess how different volumes of coagulated tissue, having different optical properties affect the imILT treatment outcome
Recursive tissue coagulation	55°C and 60°C, which are cited thresholds for thermal coagulation of biological tissue. Also by using eqs. (3.1)-(3.3)	To asses how dynamic optical and thermal properties affect the imILT treatment outcome based on the previous studies

3.2.5.1 Varying optical & thermal tissue properties

Optical and thermal properties vary between individuals and thus as well for different tumours. As a mean of investigating the impact of varying tissue properties a simulation study was performed. The thermal and optical properties were varied in a range considered realistic for *ex vivo* and *in vivo* settings in regard to bovine cardiac muscle. These tissue properties were changed one at a time. During the simulation study where the optical properties were changed, the thermal properties were fixed. They are given by table 3.2. The reduced scattering coefficient was changed within the interval 2.96 - 15.4 cm^{-1}, and the absorption coefficient was changed within the interval 0.2 - 0.4 cm^{-1}. These intervals were chosen based on data from source [36] in regard to bovine cardiac muscle tissue. Undamaged bovine cardiac muscle tissue is represented by $\mu_s' = 4.9$ cm^{-1} and coagulated tissue

is represented by $\mu_s' = 15.4$ cm^{-1}. Note that these values of the optical properties only hold for the wavelength 1064 nm.

TABLE 3.2: Thermal properties of bovine cardiac muscle. The references come in order from left to right.

ρ [kg/m^3]	c_p [J/kg·K]	k [W/m·K]	Reference
1016	3430	0.418	[37], [38], [39] + [40]

For the simulation study where the thermal properties were varied the, the heat conducitity was changed within the interval 0.197 - 0.532 W/(m·K) where 0.418 W/(m·K) is the average of the value of k from sources [39] and [40] (the values were quite scattered). Changes in density and specific heat were also simulated for, this using the intervals 993 - 1039 kg/m^3 and 3370 - 3810 J/kg·K based on values from sources [37] and [38] respectively.

3.2.5.2 Static Coagulation volumes

In addition to the optical and thermal properties varying between different patients the properties can change during treatment. These changes are induced by the increase in temperature. The most important heat induced effect is tissue coagulation. In order to investigate the impact in imILT due to different sized coagulation zones a simulation study was performed where the range of sizes for the coagulation zone was chosen to be comparable with the measured lesions from the experimental results. This range of sizes for the volume of coagulated tissue simulated for was set to 5 to 8.5 mm in diameter centred at the position of the light source. The value of μ_s' allocated to the coagulated tissue was set to 15.4 cm^{-1} and the absorption coefficient remained at 0.3 cm^{-1} as for non-coagulated tissue. The thermal properties were fixed at the values shown in table 3.2, except for one simulation were k was set to 1 W/(m·K).

3.2.5.3 Recursive tissue coagulation

Thermal coagulation of tissue is however a dynamic process where the volume of coagulated tissue develops over time dependent on heat exposure. The thermal properties of tissue also change during heat exposure, mainly due to temperature dependent dissipation of water residing in the tissue. As a mean of investigating

the impact of a dynamic change in optical and thermal properties in imILT, a simulation study was performed where these properties where recursively changed over time. The analysis of the results can be aided by the previous investigations mentioned in sections 3.2.5.1 and 3.2.5.2. The study was also performed to investigate if the model has a potential to predict the outcome of a imILT treatment. One approach to apply a dynamic dependence of the optical properties of tissue on temperature is in the form of a step function, that utilizes a threshold temperature that divides tissue into non-coagulated and coagulated, evaluated for every mesh element in the tissue geometry. The optical properties for coagulated tissue can then be dynamically allocated to the coagulated tissue regions, based on the highest temperature reached in each point. The different threshold temperatures used are 55°C and 60°C. Another approach to modulate for the dynamic changes in the optical properties due to thermal damage is by using equations (3.1)-(3.3) [35]:

$$\mu_a = \mu_{a,native} \cdot f_u + \mu_{a,coagulated} \cdot f_d \tag{3.1}$$

$$\mu_s = \mu_{s,native} \cdot f_u + \mu_{s,coagulated} \cdot f_d \tag{3.2}$$

$$g = g_{native} \cdot f_u + g_{coagulated} \cdot f_d \tag{3.3}$$

where $\mu_{a,native}$, g_{native}, and $\mu_{s,native}$ correspond to the absorption coefficient, the scattering coefficient, and the anisotropy factor of undamaged (non-coagulated) tissue respectively. The denotations $\mu_{a,coagulated}$, $g_{coagulated}$, and $\mu_{s,coagulated}$ are their counterparts in regard to coagulated tissue. The fraction of damaged tissue given by the Arrhenius equation denoted as f_d is described as $f_d(t) = 1 - \exp(-\Omega(t))$ as shown in eq. (2.8), and the fraction of undamaged tissue denoted as f_u is described as $f_u(t) = 1 - f_d(t)$. The values of the frequency factor, A, the activation energy, ΔE_a, and the universal gas constant, R, used for solving the Arrhenius equation in this thesis work are given in table 3.3. The table also contains the values used for the optical properties in this study.

TABLE 3.3: Parameters coupled to recursive tissue coagulation used in the model.

Parameter	Native tissue	Coagulated tissue	Reference
A [s^{-1}]	$2.8 \cdot 10^{23}$		[41]
ΔE_a [kJ/mole]	162 ± 9		[41]
R [kJ/(mole $\cdot$ K)]	8.314		[41]
μ_a [1/cm]	0.3	0.3	[36]
μ_s [1/cm]	140	280	[36]
g	0.965	0.945	[36]

The temperature dependence of the thermal properties of tissue can however be implemented outside of the above mentioned step function. These properties can instead be modulated as being dependent on the water content, which dissipates with temperature. An approximative description of the dynamic changes in the thermal properties of tissue in regard to water mass percentage in tissue, w, (approximately 75% for muscle tissue [42]) in the range of $20 - 100$°C is shown in equations (3.4)-(3.6) below [35]:

$$\rho(T) = 1000(1.3 - 0.3k_\rho \cdot w) \quad \left[\text{kg m}^{-3}\right] \tag{3.4}$$

$$c_p(T) = 4190(0.4 + 0.6k_{C_p} \cdot w) \quad \left[\text{J kg}^{-1}\ \text{K}^{-1}\right] \tag{3.5}$$

$$k(T) = 0.4(0.1 + 1.4k_k \cdot w) \quad \left[\text{W m}^{-1}\ \text{K}^{-1}\right] \tag{3.6}$$

where T (°C) is the tissue temperature, k_ρ, k_{c_p}, and k_k are temperature dependent factors for ρ, c_P, and k of water, and can be written as:

$$k_\rho = 1 - 4.98 \cdot 10^{-4}(T - 20°\text{C}) \tag{3.7}$$

$$k_{c_p} = 1 + 1.02 \cdot 10^{-4}(T - 20°\text{C}) \tag{3.8}$$

$$k_k = 1 + 1.78 \cdot 10^{-3}(T - 20°\text{C}) \tag{3.9}$$

Chapter 4

Results & Discussion

4.1 Ex vivo imILT experiments

Figure 4.1 shows the result from one of the imILT treatments made on bovine cardiac muscle. The line going through the circular discoloured area, the visible lesion, in the figure shows where the optical fiber was placed.

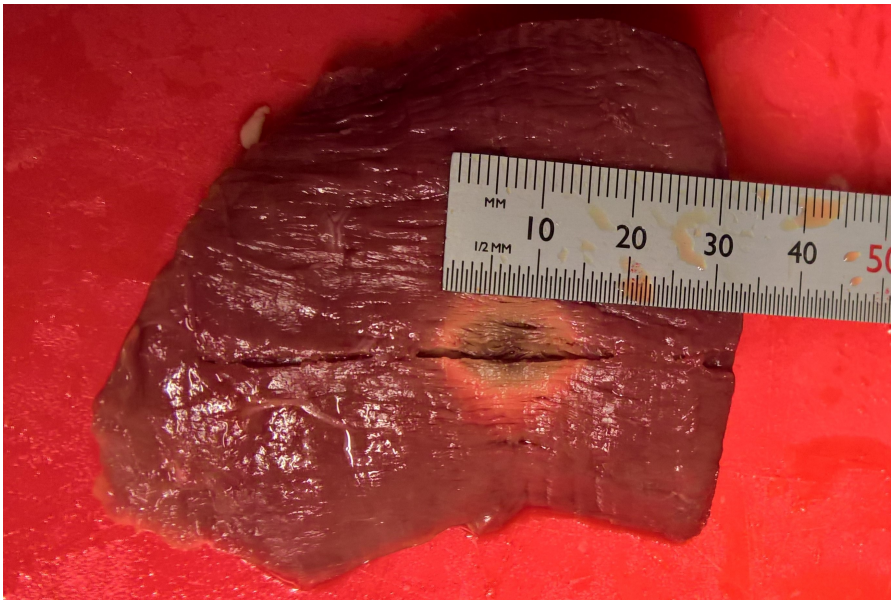

FIGURE 4.1: The result of imILT treatment 1 performed on a Bovine Cardiac muscle tissue slab, where the warm-up time was 90 s and the treatment time was 30 minutes. The discoloured area seen is the resulting lesion.

The results and evaluations from the ImILT treatment experiments made on bovine cardiac muscle are shown in table 4.1. Thirteen samples were taken from

four different hearts in total to include biological variations in the evaluation of the experiments. Treatments 5-11 in table 4.1 were made using SP1, SP2, and MP simultaneously, and thus contain temperature data at radial distances of 5, 10, and 15 mm from the fiber.

TABLE 4.1: Results and evaluations from the imILT experiments made on Bovine cardiac muscle. T_{init} is the initial temperature of the tissue, $t_{treatment}$ is the treatment time, d_{lesion} is the measured diameter of coagulated tissue in the horizontal and vertical direction, and E_{tot} is the total energy deposited into the tissue during treatment. t_{warmup} is defined as the time it takes to achieve a temperature of 46°C at the location of the master probe. Treatments 5-11 were made using SP1, SP2, and MP simultaneously. †An error in the system caused the treatment to end prematurely, this data was only used for calculations regarding the warm-up time. ⋆ The initial temperature was too low, this data was not used to calculate the standard deviation and the average of the results.

Treatment #	T_{init} [°C]	t_{warmup} [s]	$t_{treatment}$ [s]	d_{lesion} [mm]	E_{tot} [J]
1	36.0	90	1800	16×16	3124
2	37.9	82	1800	17×16	2820
3†	37.5	126	1386	(16×20)	(3140)
4⋆	34.5	(84)	1800	(14×16)	(3094)
5	35.9	130	1800	18×19	3734
6⋆	35.2	(130)	1800	(16×16)	(3694)
7	36.0	76	1800	14×13	2540
8	36.2	100	1800	14×16	2880
9	37.6	42	1800	9×9	1960
10	36.2	54	1800	11×11	2086
11	36.5	158	1800	19×20	4124
12	37.2	92	1800	12×14	2620
13	37.1	102	1800	14×14	2860
STD		33.6		3.2×3.6	666.7
Average		95.6		14.4×14.8	2875

The resulting temperature curves measured by the master probe for the first 230 s for treatments 1-13 are shown in figure 4.2. temperature curves measured by the master probe for the treatments tabulated in table 4.1 that generated the slowest, most average, and fastest warm-up time respectively. The additional temperature

data obtained from treatments 5-11 for the 5 and 15 mm source-probe distances are shown in figures 4.3 and 4.4, respectively.

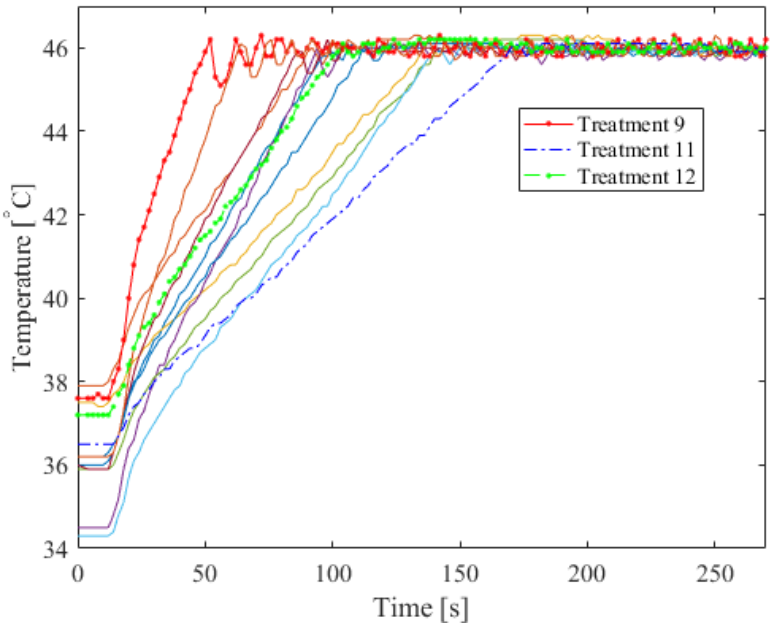

FIGURE 4.2: The resulting temperature curves for the imILT treatments, 1-13, for the first 270 s measured by the temperature probe located 10 mm from the radial fiber. The Emphasized temperature curves representing treatments 9, 11 and 12 resulted in the shortest, longest, and most average warm-up time respectively.

From figure 4.2 it can be seen that the temperature curves appear to have a linear relationship with time during the warm-up time, where the size of the gradient has a possible tendency to increase with increasing initial temperature. This possible dependency of the gradient on the initial temperature is however undermined in regard to the diversity of the treatment outcomes, shown in table 4.1, for which there is e.g. a large discrepancy regarding treatments 3 and 9 where the initial temperature of the tissue slabs differed by 0.1°C. This is likely due to biological variations between the tissue samples. The difference in the warmp-up time between the treatments corresponds to a standard deviation of 33.6 s which in turn corresponds to about 35% of the average warm-up time of 95.6 s. The measured area of coagulated tissue for treatments 1-13 shown in table 4.1 appears to be in some extent dependent on the warm-up time, which in the case of treatments 5-11 corresponds to a higher temperature at a distance of 5 mm from the light source, as shown in figure 4.3. The total energy deposited into the tissue slabs during the treatments in conjunction with the initial temperature of the tissues might

determine the size of the lesion, where a larger total energy together with a lower initial temperature seems to yield a larger lesion size.

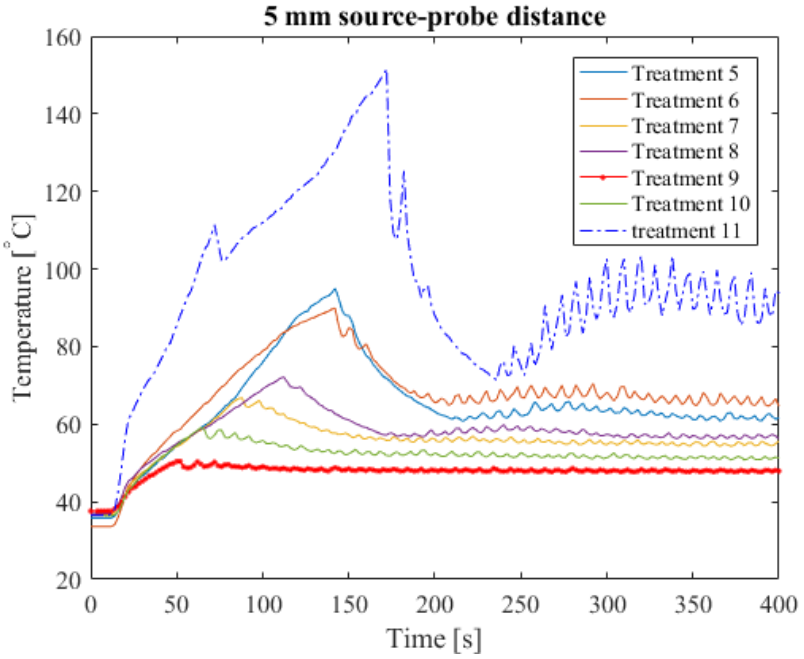

FIGURE 4.3: The resulting temperature curves from the imiLT treatments 5-11 from table 4.1, for the first 400 seconds, measured by a temperature probe located 5 mm away from the radial fiber. The solid temperature curves come in order (in regard to the legend) from the highest peak to the lowest.

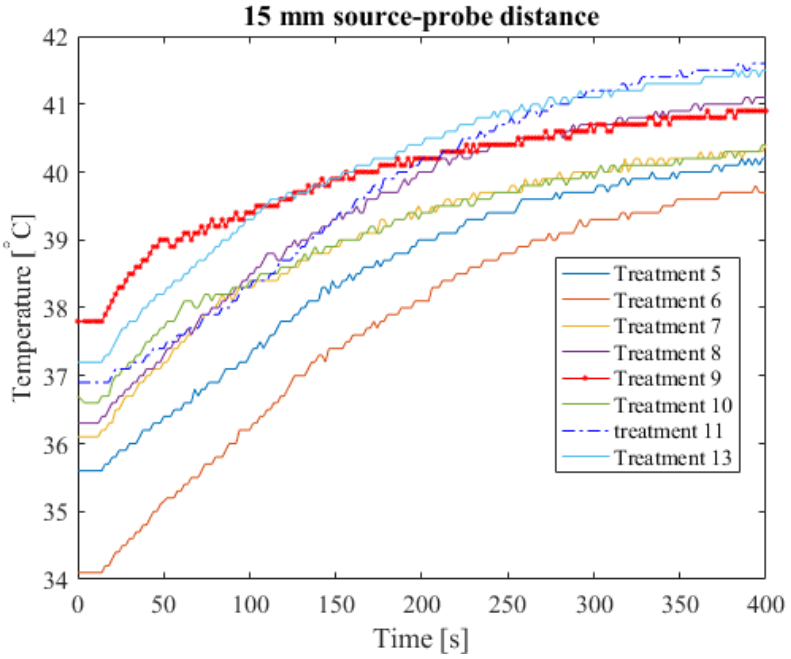

FIGURE 4.4: The resulting temperature curves from the imiLT treatments 5-11 from table 4.1, for the first 400 seconds, measured by a temperature probe located 15 mm away from fiber.

Treatments 2-5, 7, 8, 11 and 12 resulted in elongated lesions which might indicate that the lesions follow the direction of the muscle fibres observed in the tissue slabs, which e.g. can be seen in figure 4.1. This would possibly introduce an environment with different optical and thermal interactions, and therefore possibly provide a higher level of uncertainty between the experiments. Liquid in the tissue might also move easier along the muscle fiber which further affects the heat conductivity, and contributes to a more elongated lesion. Regarding the faster warm-up times seen for treatments 9 and 10 in table 4.1 a possible error might be caused by the placement of the optical fiber and and the master probe. The master probe was seen to have a slight tilt towards the optical fiber, decreasing the distance between them.

In general there are a number of possible sources of errors regarding the experimental procedure and the tissue used, which might be related to a difference in optical and thermal properties for the tissues used, and also how the optical fiber and the master probe were placed in relation to each other. The different bovine hearts that the tissue samples where cut from looked physically different. For example, in colour, the amount and size of blood vessels, and in porosity. The

colours differed in the reddish tone, and this is in part connected to the amount of blood left in the tissue. This would imply a possible difference in light absorption between the hearts cut since a larger concentration of blood would increase the amount of absorbed light closer to the fiber. The blood vessels were avoided during the treatments, but the small holes in the tissues accompanied with the porosity were difficult to avoid. These holes might have induced errors in the treatments as they would for example introduce inhomogeneous regions within the tissue, possibly contributing to different local scattering and thermal properties. These holes would thus affect the light distribution and therefore alter the treatment outcome. Liquid might also be more movable in the holes, and would then generate an increase in heat transfer, resulting in a larger uncertainty in the treatment outcome.

As mentioned earlier, errors due to inaccurate placement of the optical fiber and the master probe also induces uncertainties in the treatments. They might have been shifted in height from the planned depth or in the horizontal direction. If the distance between them decreases the warm-up time would also decrease as the laser-induced heat introduced in the tissue would be needed to be transported a smaller distance. Another effect on the treatment outcome is the possibility of tissue carbonization which might occur during the treatment. Carbonized tissue is a greater absorber of light than undamaged or coagulated tissue and therefore shortens the distance light can travel in the tissue. This would introduce a steeper heat gradient generated by absorption in the tissue. Carbonization reduces the efficiency of the feedback process since the energy deposited in the tissue is transported to the point where the temperature is measured with a delay. Therefore, carbonized tissue might imply that a higher amount of total laser light deposited into the tissue is required for the treatment. Carbonized tissue was not directly observed during the experiments, but rather a beginning of carbonization was seen. The part of the tissues closest to the fiber in the experiments looked dehydrated and had a dark brown tone, which seemed to differ from normal coagulated tissue. This would, following an argument similar to that concerning carbonization, possibly affect the treatment outcome. This area of dehydrated tissue differed in size between the experiments and were more profound for treatments with longer warm-up times. This could be a possible contributor to the difference in lesion size between the treatments.

In regard to treatment 12, which has a warm-up time closest to the average time

of 92 s, a graph of the accompanying laser power modulation is shown in figure 4.5 to be compared with the simulation model developed in this thesis.

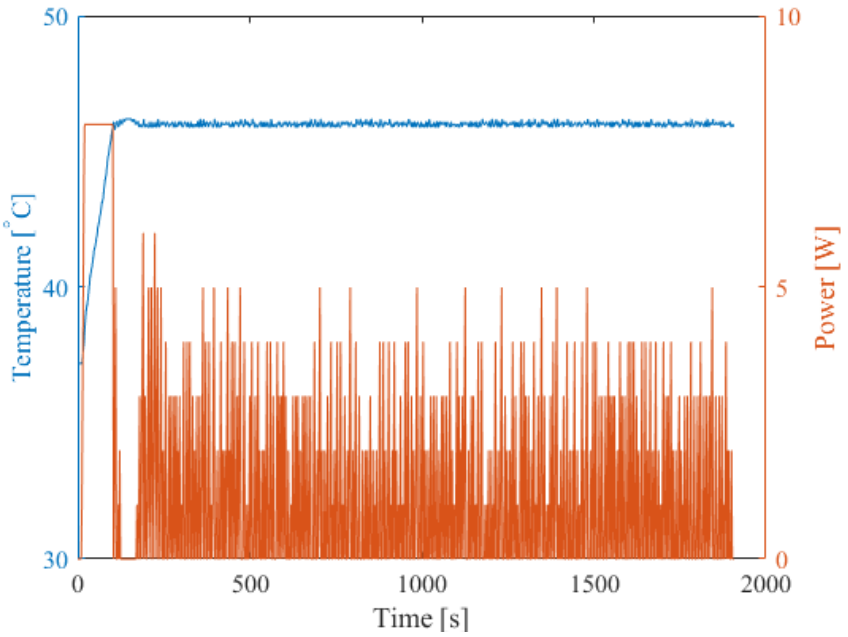

FIGURE 4.5: The temperature curve for treatment 12 with the corresponding laser output power graph, both plotted for the treatment time plus the warm-up time (a duration of 1892 s).

4.2 Simulations of imILT

4.2.1 Varying optical & thermal input parameters

The results from the experiments performed in this thesis presented in section 4.1 were scattered which implies the importance of conducting an investigative simulation study of for example varying optical and thermal properties of tissue. The absorption coefficient and the reduced scattering coefficient are important factors in laser-induced interstitial thermotherapy since they govern the light distribution in tissue. This affects the heat distribution generated in tissue due to light absorption, and is thus also a governing factor in the amount of optical energy that is required to keep the tissue temperature at 46°C at the tumour border. Theoretical simulations were performed in order to investigate how significantly a variation in the optical properties affects a treatment, where the optical properties were varied in a range considered realistic for *ex vivo* and *in vivo* settings. The

thermal properties of tissue might also vary between tissue samples which would affect how the temperature is distributed throughout the tissue. Similar imILT simulations were thus also made for varying thermal properties.

4.2.1.1 Varying optical parameters

The power modulation of the light source given when simulating for bovine cardiac muscle parameters is shown in figure 4.6.

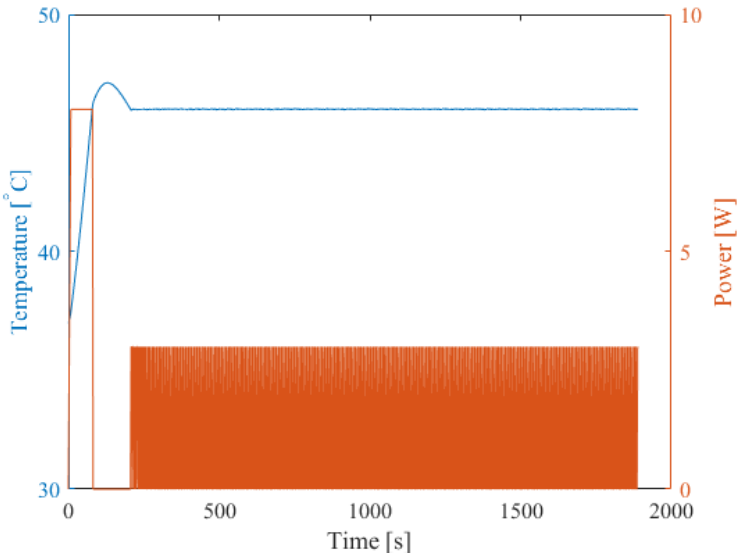

FIGURE 4.6: The simulated output power from the light source in bovine cardiac muscle accompanied with the temperature measured at the master probe, both plotted for the treatment time plus the warm-up time (a duration of 1880 s).

The generated temperature plots at 5, 10 and 15 mm from the source when varying the absorption coefficient, μ_a, are shown in figures 4.7 (a), 4.7 (b) and 4.7 (c) respectively.

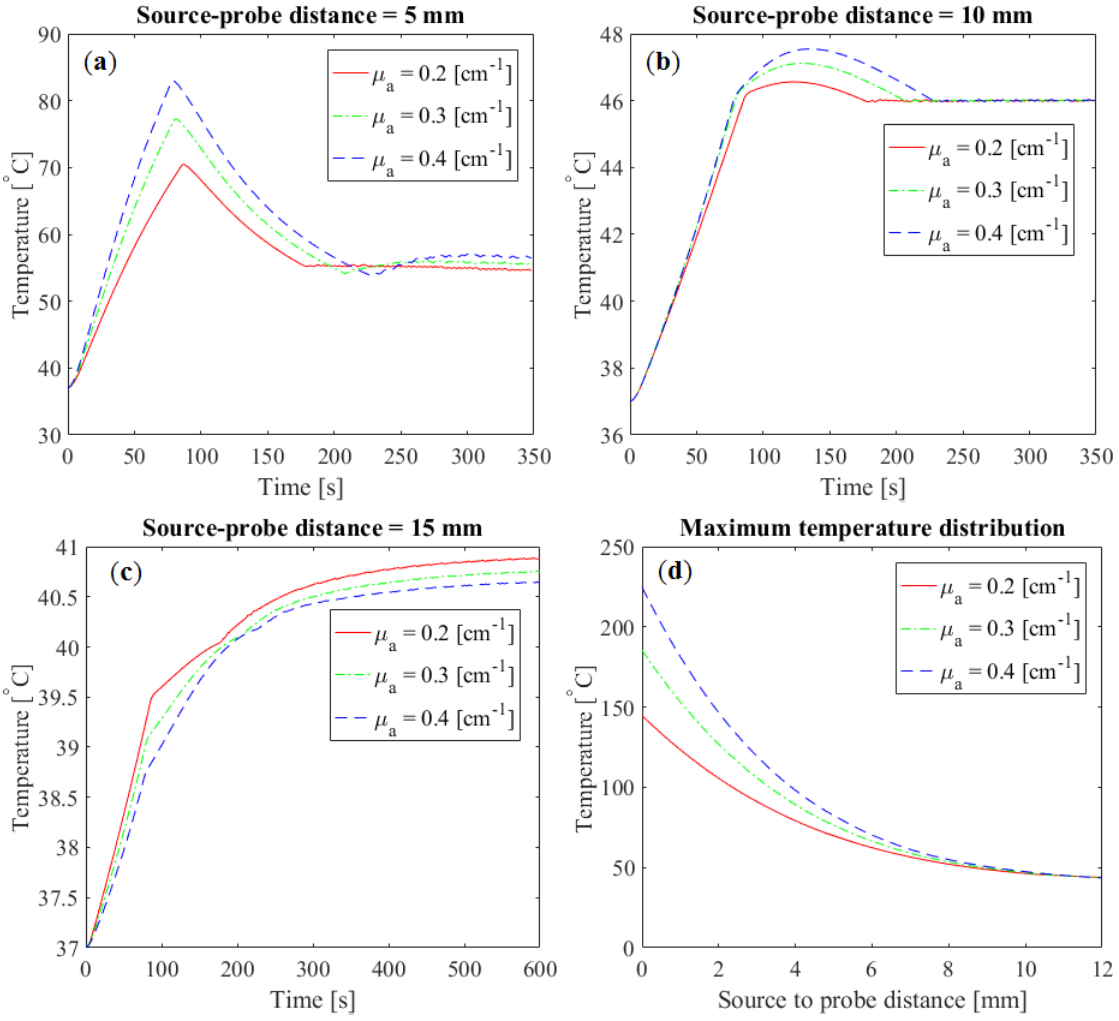

FIGURE 4.7: The resulting temperature data from imILT treatment simulations of bovine cardiac muscle tissue where the absorption coefficient has been varied from 0.2 to 0.4 cm^{-1}. (a), (b), and (c) show the measured temperature over time before temperature stabilization at distances of 5, 10, and 15 mm away from the light source respectively. (d) shows the temperature maximum distributions in one direction from the light source to a point 12 mm away.

Comparing the simulated results shown in figure 4.7 to the experimental results shown in figures 4.2-4.4, it was observed that the results of the simulated treatments fall into the range of the experiments. This implies that the simulation model might yield relevant results when investigating the impact in imILT due to changes in optical and thermal properties. From figure 4.7 (b), regarding the master probe, it can be seen that a higher absorption coefficient heats the tissue to the target temperature of 46°C at a faster rate, as well as inducing a higher temperature overshoot above the target temperature. A similar analysis can be made for the results regarding a 5 mm source-probe distance (figure 4.7 (a)), where the

temperature rises at a faster rate for a higher absorption coefficient and reaching a higher maximum temperature. This trend is however, as expected, broken at a distance of 15 mm from the light source, where the opposite behaviour is seen. A probable reason for this is coupled to optical penetration, where a larger μ_a results in a greater localization of the optical energy, yielding a more localized heat source. This would also imply a higher total energy in a region closer to the source, yielding a higher temperature in this region, which furthermore, in regard to heat transfer, would result in a higher rate of heat transport to tissue regions further away. This might explain the faster rate of heating for a larger μ_a as seen in figures 4.7 (b) and 4.7 (a), but as the distance increases between the point of temperature measurement and the source, as for the case in figure 4.7 (c), this argument is no longer observed to be fulfilled, which might be due the limitation on heat transport in relation to the temperature gradient introduced in the tissue via absorption. The difference in temperature overshoot seen in figure 4.7 (b) is therefore possibly coupled to the distribution of the heat source, where a more distributed heat source yields a faster feedback process due to a decrease in the delay of the transportation of optical energy (as mentioned in section 4.1). Thus a larger μ_a leads to a larger temperature overshoot above 46°C at the master probe distance.

The maximum temperature distribution in one direction from the light source to a point 12 mm away for the three simulations where μ_a was varied, are shown in figure 4.7 (d). From the figure, it can be seen that the temperature difference between the three curves decreases with the distance from the light source, until a point where they intersect and the relation becomes inverted (barely seen in the figure). The temperature is as expected higher towards the light source for the curve where $\mu_a = 0.4$ cm^{-1}. The explanation for the seen difference in temperature between the curves in the figure might concur with the argument given for the results shown in figures 4.7 (a)-4.7 (c) in regard to the dependency of the localization of the optical energy on μ_a, and the accompanying effects on heat transfer.

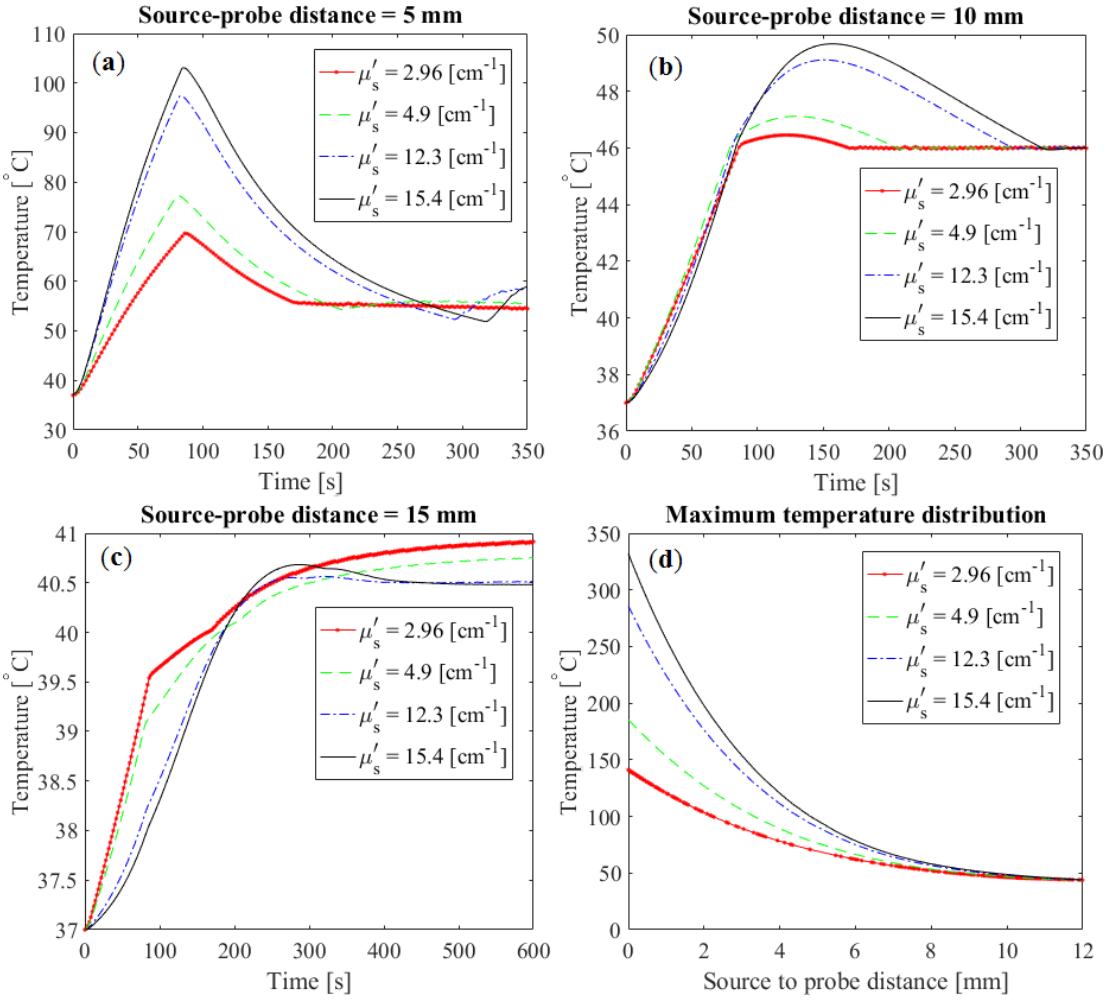

FIGURE 4.8: The resulting temperature data from imILT treatment simulations of bovine cardiac muscle tissue as a result of changing μ_s' between 2.96, 4.9, 12.3, and 15.4 cm^{-1}. (a), (b), and (c) show the measured temperature over time before temperature stabilization at distances of 5, 10, and 15 mm away from the light source respectively. (d) shows the maximum temperature distributions in one direction from the light source to a point 12 mm away.

The measured temperature data obtained when changing the reduced scattering coefficient, μ_s', is shown in figure 4.8. Regarding the change in μ_s' it can be seen from figures 4.8 (a)-4.8 (c) that an increase in the reduced scattering coefficient induces a similar behaviour as for an increase in the absorption coefficient. The overshoot in temperature above 46°C also appears to increase with an increase in μ_s'. When it comes to the characteristics of optical scattering, a higher scattering coefficient implies a higher probability for a more localized light distribution, due to the probability of more scattering events for a shorter distance, which appears to be in good correlation with the results. The different temperature distributions shown in figure 4.8 (d) are as in the case of varying μ_a showing a possible correlation

between the maximum temperature at an arbitrary point and the value of the scattering coefficient, for which a larger μ_s' results in a higher temperature for a certain distance away from the source. This is however limited by the size of the temperature gradient induced into the tissue (as described for varying μ_a) and the localization of the optical energy, which to some extent can be seen in figure 4.8 (c).

The results and evaluations generated by the imILT simulations where μ_a and μ_s' were varied are shown in table 4.2. It can be seen from the table that a higher value of μ_a gives a larger temperature overshoot above 46°C, a longer cool-down time, a larger lesion diameter, and a smaller amount of energy deposited into the tissue (E_{tot}). An increase in μ_s' yields similar results. This is similarly seen for the reduced scattering coefficient, μ_s'. A possible reason for this phenomenon might be correlated to the size of the introduced temperature gradient together with the localization of the optical energy and heat transfer. Here, a larger temperature gradient could imply a temperature distribution with a higher minimum temperature (due to heat transfer), which might result in a lower amount of optical energy needed to warm the tissue back to 46°C after turning off the heat source. It can furthermore be seen from the results that the significant differences between the simulations occur during the warm-up time, which is influenced by the tissue properties investigated. When it comes to the significance of a change in optical properties for a treatment, the absorption coefficient, albeit the smaller range in input parameters in regard to the reduced scattering coefficient, almost has a comparable impact on the treatment outcome. The reduced scattering coefficient is however the parameter out of these two that is said to change the most during a treatment, which is mainly due to tissue coagulation, where the value of μ_s' approximately doubles, and induces a noticeable change on the treatment outcome, seen by the results of the simulations.

TABLE 4.2: Results and evaluations from the imILT simulations made on Bovine cardiac muscle when varying μ_a and μ_s'. Here, the warm-up time is denoted as t_{warmup}, the temperature reached above 46°C (overshoot) is represented by T_{os}, the time it took for the tissue temperature to decrease to 46°C after the overshoot is denoted $t_{cooldown}$, the accumulated lesion size (zone of coagulation) is written as d_{lesion}, and E_{tot} is the total energy deposited into the tissue during treatment.

μ_a [1/cm]	μ_s' [1/cm]	t_{warmup} [s]	T_{os} [°C]	$t_{cooldown}$ [s]	d_{lesion} [mm]	E_{tot} [J]
0.2	4.9	86	0.6	92	14.6	2944
0.3	4.9	80	1.1	128	15.3	2584
0.4	4.9	78	1.5	150	15.8	2388
0.3	2.96	86	0.5	84	14.5	2980
0.3	12.3	82	3.1	212	16.4	2258
0.3	15.4	84	3.7	234	17.0	2190

4.2.1.2 Varying thermal parameters

The results of the simulated temperature curves at distances of $5, 10$ and 15 mm away from the light source generated when changing the heat conductivity, k, are shown in figure 4.9. A plot of the accompanying maximum temperature distributions to a point located 12 mm away from the light source is shown in figure 4.9 (d). It is from figure 4.9 noticeable that a higher conductivity results in a more uniform heat distribution, which is in correlation with the lower maximum temperature observed. A higher value of k also demonstrates a faster heat transport throughout the tissue, which can be seen in figure 4.9 (c) where the temperature is measured 15 mm away from the point source. The faster rate of heat transfer seen when increasing heat conductivity gives a possible explanation for the difference in the temperature overshoot above 46°C between the temperature curves in figure 4.9 (b).

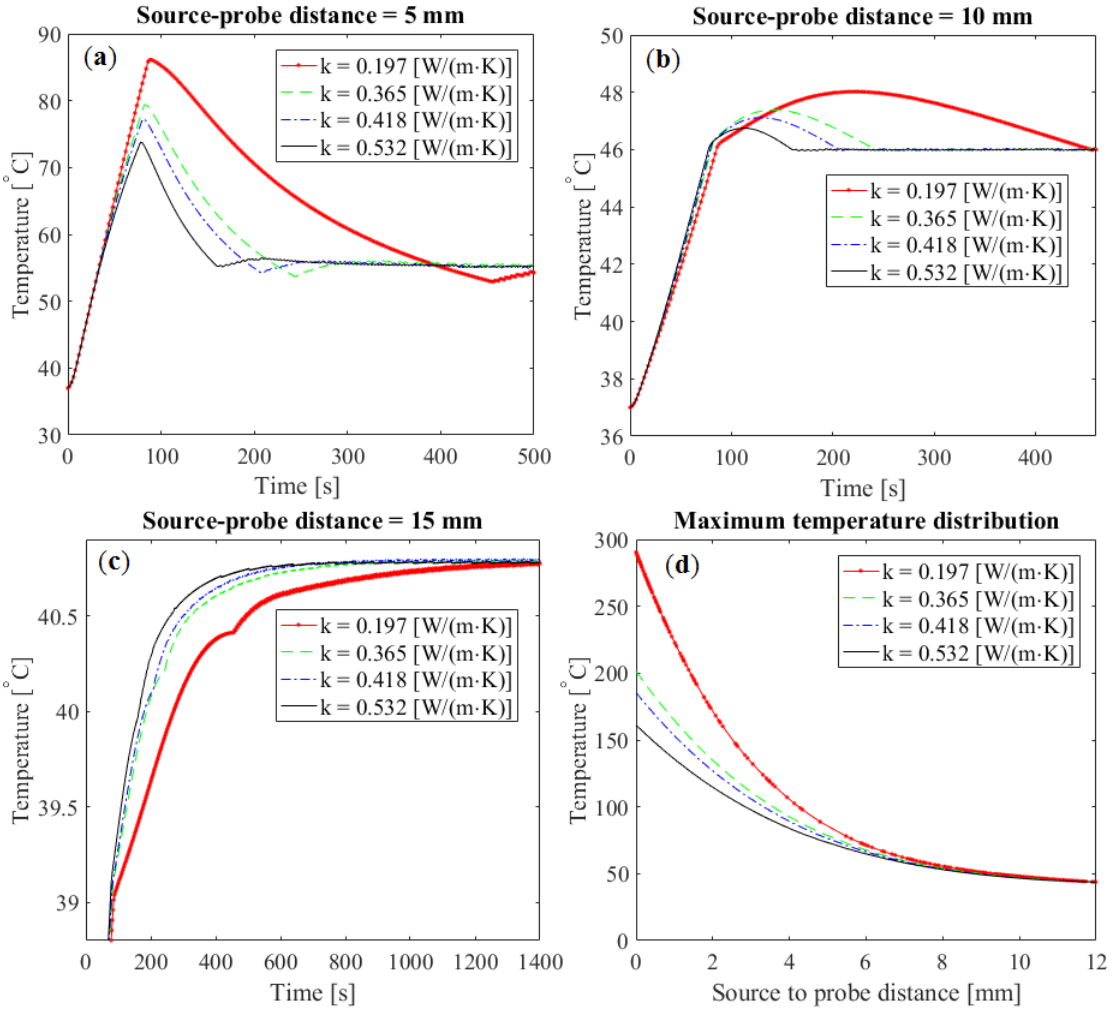

FIGURE 4.9: he resulting temperature data from imILT treatment simulations of bovine cardiac muscle tissue where the heat conductivity has been varied from 0.197 to 0.532 W/(m·K). (a), (b), and (c) show the measured temperature over time before temperature stabilization at distances of 5, 10, and 15 mm away from the light source respectively. (d) shows the temperature maximum distributions in one direction from the light source to a point 12 mm away.

A summary of the results and evaluations from the imILT simulations in regard to varying the thermal properties is given in table 4.3. The volume of coagulated tissue decreases with an increase in conductivity, which in this case is a direct relation to the the temperature distribution seen in figure 4.9 (d) since 55°C was the temperature used to separate undamaged tissue from coagulated. Changes in the total energy deposited into the tissue between the treatments seems to increase with an increase in heat conductivity. The results from the simulations performed to investigate the effect on a treatment when varying the density, ρ, and the specific heat c_p seen in table 4.3, do not vary in the same magnitude as the

results obtained when varying the heat conductivity. This can be seen from the evaluation of the lesion size and the total energy deposited into the tissue where the difference is very small. The effect on the treatment outcome when changing the heat conductivity is of greater importance, and the size of variation of the cited values for this parameter in regard to bovine cardiac muscle yields a significant effect to end result of a treatment.

TABLE 4.3: Results and evaluations from the imILT simulations made on Bovine cardiac muscle when varying k, ρ, c_p. Δ thermal property represents the thermal property being changed, the warm-up time is denoted as t_{warmup}, the temperature reached above 46°C (overshoot) is represented by T_{os}, the time it took for the tissue temperature to decrease to 46°C after the overshoot is denoted $t_{cooldown}$, the accumulated lesion size is written as d_{lesion}, and E_{tot} is the total energy deposited into the tissue during treatment.

Δ Thermal property	t_{warmup} [s]	T_{os} [°C]	$t_{cooldown}$ [s]	d_{lesion} [mm]	E_{tot} [J]
$k = 0.197$ W/(m·K)	86	2.0	370	16.2	1486
$k = 0.365$ W/(m·K)	82	1.4	162	15.6	2312
$k = 0.418$ W/(m·K)	80	1.1	128	15.3	2584
$k = 0.532$ W/(m·K)	78	0.7	182	15.1	3126
$\rho = 993$ kg/m^{-3}	78	1.1	122	15.3	2562
$\rho = 1039$ kg/m^{-3}	82	1.1	130	15.3	2588
$c_p = 3370$ J/(kg·K)	78	1.0	120	15.3	2562
$c_p = 3810$ J/(kg·K)	88	1.0	138	15.3	2636

4.2.2 Discussion about changing the medium to be treated

Changing to another tissue type or to another tissue state (for example if the tissue is frozen) in the model is equivalent to changing the optical and thermal parameters in the model. Bovine Liver tissue for example has a lower absorption coefficient, a higher μ_s', and a higher heat conductivity than than Bovine cardiac muscle tissue [36],[39]. If the parameters in the model are changed to the ones of another tissue type, the change in the simulation results would be foreseeable based on the the results obtained in the parameter-changing study. Changing the tissue state to coagulated is also important to investigate since the process of thermal coagulation of tissue occurs during imILT, which in the model is done by changing the optical parameters and thermal parameters to that of the coagulated tissue of interest. This is also done when recursively implementing coagulated

tissue in the model. The results from the model implemented in this thesis are furthermore shown in sections 4.2.3 and 4.2.4.

4.2.3 Introducing static Coagulation volumes

As seen from the results in section 4.2.1.1, the change in optical properties due to tissue coagulation are significant, and if a simulation model more comparable to *ex vivo* imILT experiments is desired, the model needs to contain conditions for both non-coagulated and coagulated tissue. Therefore, simulations of imILT where a certain volume of coagulated tissue was introduced in the model were performed. The size of the volume of coagulated tissue was changed between the simulations as a mean of further investigating the effects on the treatment outcome. The results of these simulations in regard to the measured temperature data are shown in figure 4.10.

From the results given in figure 4.10 (b) there is a considerable difference in warm-up time between non-coagulated bovine cardiac muscle tissue and coagulated tissue, which is an attribute of the increase in scattering in the region of the tissue model where the tissue is determined to be coagulated. The effect on the treatment when increasing the reduced scattering coefficient, as discussed in section 4.2.1.1, gives a more localized light distribution and thus a larger temperature gradient, which can be seen in figure 4.10 (d). The size of the coagulation volume is however an important factor since light is less efficiently scattered in the non-coagulated tissue outside the coagulated volume. This implies that the part of the already diffused light escaping the coagulated volume becomes scattered over a more widespread volume and is absorbed quickly. This is due to the difference in the scattering properties between non-coagulated and coagulated tissue. It can furthermore be seen from the results in figure 4.10 that heat transport due to thermal properties is a slower process than heat generation due to the absorption of light. This can be seen by the high overshoot in temperature above 46°C together with higher temperatures closer to the light source when a volume of coagulated tissue is introduced in the simulation model. An increase in heat conductivity can however have a significant impact on heat transfer which can be observed in figure 4.10. This in regard to the case where $k = 1$ W/(m·K) within a coagulation volume of 5 mm in diameter, where in comparison to the simulation where $k = 0.418$ W/(m·K) and $d_c = 5$, the warm-up time has decreased by 10 s, the temperature

closest to the light source is lower, and the temperature at a distance of 15 mm away from the light source increases almost as fast as for non-coagulated tissue.

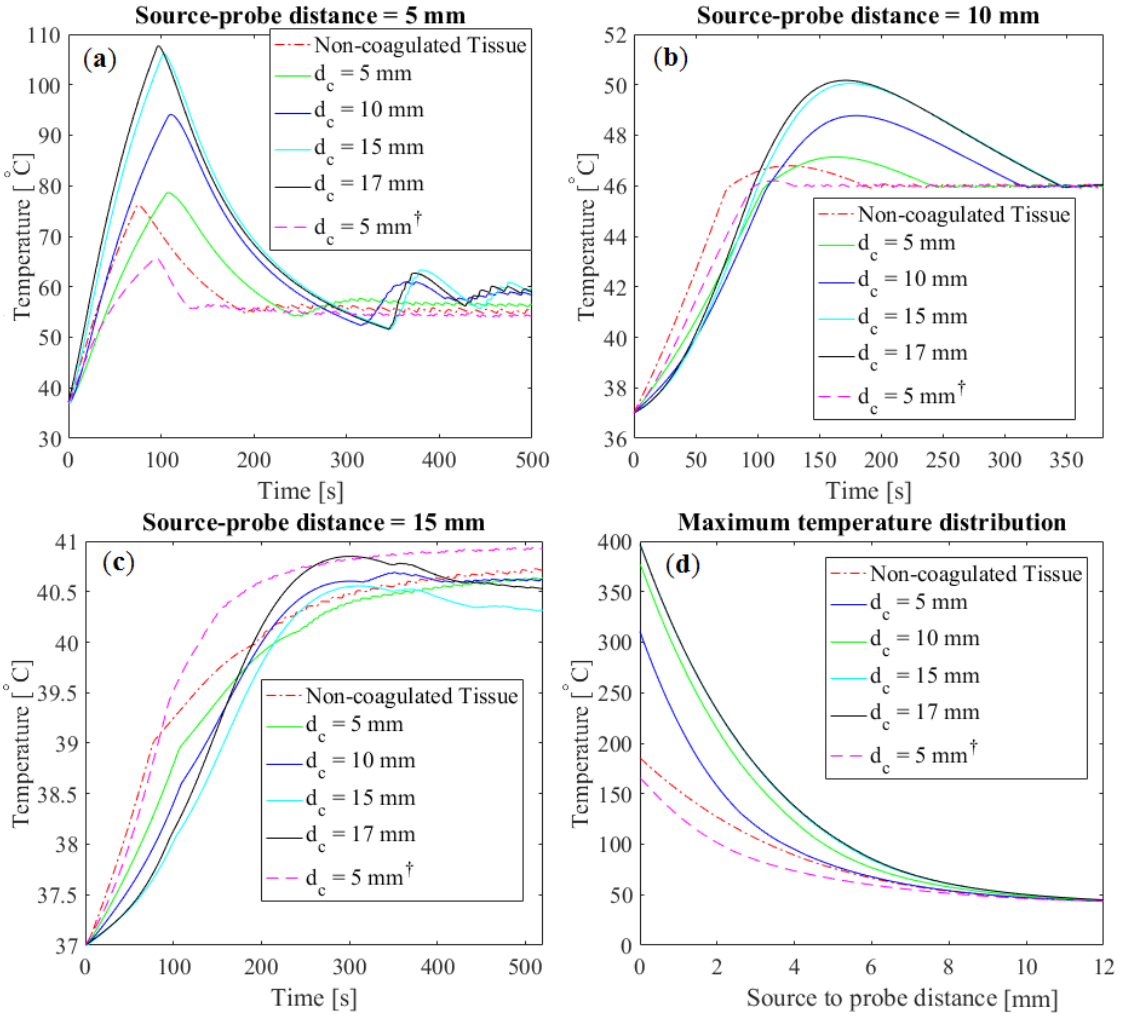

FIGURE 4.10: The resulting temperature data from imILT treatment simulations of bovine cardiac muscle tissue where coagulation zones of 5-17 mm in diameter have been introduced. (a), (b), and (c) show the measured temperature over time before temperature stabilization at distances of 5, 10, and 15 mm away from the light source respectively. (d) shows the temperature maximum distributions in one direction from the light source to a point 12 mm away. † $k = 1$ W/(m·K) for coagulated tissue.

The results and evaluations of the imILT simulations where different sized coagulation zones were introduced in the tissue are shown in table 4.4.

TABLE 4.4: Results and evaluations from the imILT simulations made on Bovine cardiac muscle when varying the diameter of coagulated tissue, d_c. Here, t_{warmup} is the warm-up time, the temperature reached above 46°C (overshoot) is represented by T_{os}, the time it took for the tissue temperature to decrease to 46°C warm-up is denoted $t_{cooldown}$, and the accumulated lesion size (zone of coagulation) is written as d_{lesion}. † $k = 1$ W/m(·K) for coagulated tissue.

d_c [mm]	t_{warmup} [s]	T_{os} [°C]	$t_{cooldown}$ [s]	d_{lesion} [mm]
0	80	1.1	128	15.3
5	108	1.1	134	15.6
10	110	2.8	204	16.9
15	101	4.1	246	17.8
17	97	4.2	248	17.7
5†	98	0.197	32	14.0

Comparing the simulated static coagulation volumes with the experimental results in section 4.1, the simulation having $d_c = 17$ mm lies closest to the experimental results in regard to the average warm-up time of 95.6 s, but gives however, an overestimation in the lesion size in regard to the average lesion size of approximately 15 mm in diameter from the experiments. The lesion size generated when only using parameters for non-coagulated tissue is however closer in agreement with the experimental results. The maximum temperature distribution close to the point source achieved when simulating for $d_c = 17$ mm is close to temperatures of 400°C, which are temperatures probable of inducing tissue carbonization. Carbonized tissue was however, not seen during the experiments. Furthermore, the temperature overshoot above 46°C at the master probe for the experiments did not go beyond 0.5°C. Albeit these differences in the treatment outcome between the experimental results and the model, the results from the model lies within the range of the results from the experiments, and the temperature curves show a similar behaviour and contain a similar temperature interval as the experiments. This indicates that a simulation model of imILT implementing a static coagulation zone of a certain size might give a good estimation of an *ex vivo* treatment outcome, but can in general only be used for post-experimental analysis. This since the introduced coagulation zone is a parameter found by best fit with experimental results.

4.2.4 Recursive tissue coagulation

It is discussed in section 4.2.3 that there is a significant difference in warm-up time and temperature distribution whether or not coagulation is considered. For the simulations where thermal coagulation was considered in the form of a fixed volume the resulting warm-up times were closer to that of the average warm-up time of 95.6 s seen for the experiments in section 4.1. The optical properties were changed for a chosen fixed region where tissue was deemed coagulated at all times, but this simplification is however not a dynamic process. In reality, the changes in the properties of tissue during heating is a dynamic process dependent on heat exposure and exposure time. The thermal properties of tissue coupled to the bioheat equation have been fixed at all times for the previous simulations in this thesis work. This might induce an effective error to the results since the thermal properties of tissue are said to be predominately dependent on the temperature in terms of water content. Water contained in tissue dissipates during heat exposure and an approximate description of water dissipation correlated to the thermal properties is shown in equations (3.4)-(3.6) in section 3.2.5.3. As from the results in section 4.2.1.2, a shift in the value of heat conductivity can have a significant impact on heat transfer. The temperature dependency of heat conductivity is therefore also an important parameter to be taken into consideration.

To more accurately mimic the true scenario following laser induced thermotherapy, a simulation model taking into account dynamic changes of tissue optical and thermal properties was developed. Following this, simulations of imILT were performed with the implementation of two separate dynamic determination methods simultaneously. One method for the thermal properties of tissue (eqs. (3.4)-(3.6)) and one for the optical properties. The dynamic changes in the optical properties of tissue were changed either by using the temperature thresholds 55°C and 60°C separating non-coagulated and coagulated tissue, or by using the equations (3.1)-(3.3) based on the Arhenius equation. The optical properties simulated for, as well as the activation energy and the frequency factor used in the Arrhenius equation are summarized in table 3.3 in section 3.2.5.3.

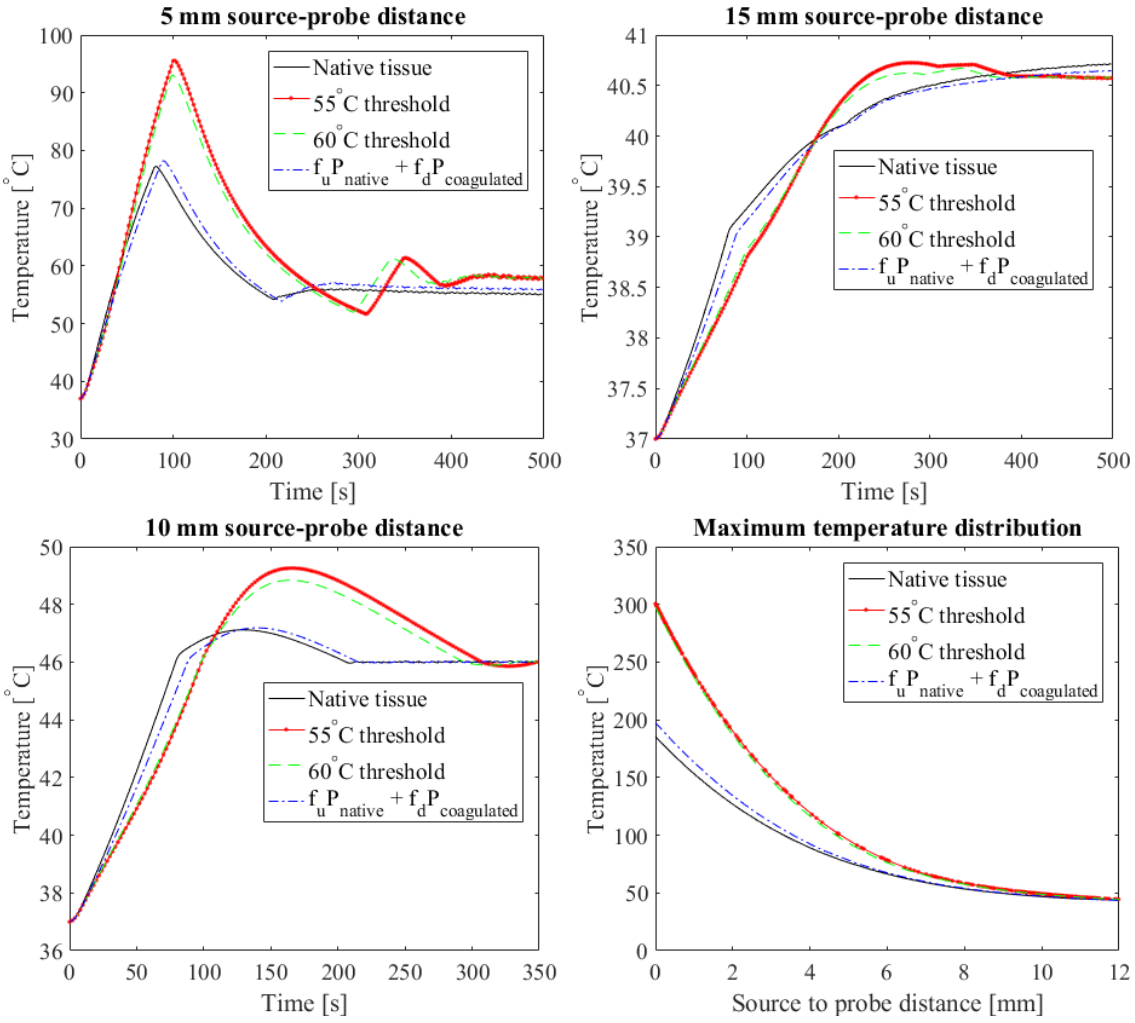

FIGURE 4.11: The resulting temperature data from imILT treatment simulations of bovine cardiac muscle tissue where recursive tissue coagulation has been implemented. P_{native} and $P_{coagulated}$ represents the optical properties for native and coagulated bovine cardiac muscle tissue respectively. (a), (b), and (c) show the measured temperature over time before temperature stabilization at distances of $5, 10$, and 15 mm away from the light source respectively. (d) shows the temperature maximum distributions in one direction from the light source to a point 12 mm away.

The results from the simulations where recursive tissue coagulation was implemented in the model, are in regard to the measured temperature data shown in figure 4.11. The simulations utilizing a threshold of either 55°C and 60°C to recursively determine tissue coagulation gave similar results. The small difference between these two is seen regarding the maximum temperature peak in figures 4.11 (a),(b), and (c). This difference is related to the threshold temperature for which the volume of tissue with altered properties increases faster when implementing the lower threshold temperature. These simulations yield results similar to that

when implementing a coagulation volume of 10 mm in diameter. The temperatures achieved when using the fraction of damaged, f_d, and undamaged tissue, f_u, to determine the change in optical properties are closer to the simulation where the tissue properties were unchanged. A reason for the difference between the simulated results where the optical properties have been changed dynamically either using the Arrhenius eq. or a temperature threshold is that the tissue region reaching the threshold temperature is altered directly, while this is not the case when implementing the Arrhenius equation. This equation determines the tissue damage in terms of temperature and time and therefore leads to changes in optical properties closer to the light source at a slower pace than the previous approach.

A summary of the results and evaluations from the simulations were the tissue properties were dynamically changed throughout the treatment are shown in table 4.5. The warm-up time from the results lie close to the average value of the warm-up time from the experiments, where this time for the simulations using a threshold temperature to determine tissue coagulation is slightly longer, 4.4 s using 55°C and 2.4 s using 60°C. When using the fraction of damaged and undamaged tissue calculated from the Arrhenius eq. as an indicator for the change in the tissue optical properties, the warm-up time is 7.6 s shorter. Considering the calculated lesion size for the three different simulations the one using a temperature threshold of 60°C to determine tissue coagulation has the lesion size closest to the average from the experiments differing by +0.22 mm in width and −0.18 mm in height. Using 55°C as a temperature threshold might give an overestimation of the lesion size. The total deposited energy in the tissue resulting from the simulations using a temperature threshold for thermal coagulation have values lower but close to the experimental data. Regarding the results of implementing a dependence for the optical properties on the fraction of damaged and undamaged tissue, the lesion size and the total energy deposited into the tissue can partly be analysed since the simulation had to be aborted after 1666 s. This due to a convergence error in the model solver. It can however be estimated that during the remaining 222 s the lesion size would increase to about 14 mm in diameter and the total energy deposited into the tissue would be about 2756 J. These estimations are only statistical and might not be applicable, but if they are reproducible they yield values close to the average of the experimental results.

TABLE 4.5: Results and evaluations from the imILT simulations made on Bovine cardiac muscle when implementing recursive tissue coagulation by the means of a threshold. Here, t_{warmup} is the warm-up time, the temperature reached above 46°C (overshoot) is represented by T_{os}, the time it took for the tissue temperature to decrease to 46°C after the overshoot is denoted $t_{cooldown}$, the accumulated lesion size is written as d_{lesion}, and E_{tot} is the total energy deposited into the tissue. The fraction of undamaged and damaged tissue are represented by f_u and f_d respectively. The expressions P_{native} and P_{coag} represents the optical properties for native (non-coagulated) and coagulated bovine cardiac muscle tissue respectively.† the simulation had to end after 1666 s due to a convergence error in the model solver.

Coagulation threshold	t_{warmup} [s]	T_{os} [°C]	$t_{cooldown}$ [s]	d_{lesion} [mm]	E_{tot} [J]
55 [°C]	100	3.26	208	17.13	2634
60 [°C]	98	2.84	196	14.62	2524
$(f_u P_{native} + f_d P_{coag})^{\dagger}$	88	1.19	128	12.99	2438

A 2D temperature map from the simulation using a 60°C threshold for thermal coagulation of bovine cardiac muscle is shown in figure 4.12.

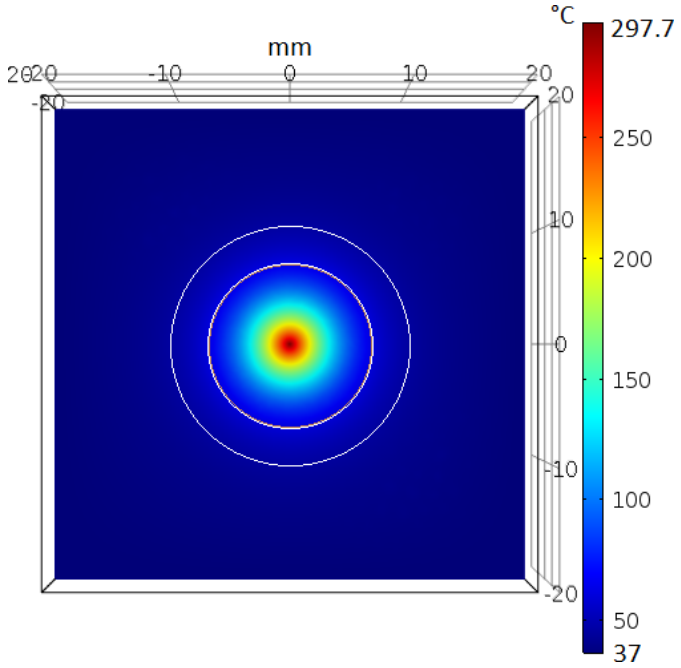

FIGURE 4.12: The simulated 2D temperature map obtained when implementing recursive coagulation of bovine cardiac muscle tissue using a 60°C threshold for tissue coagulation. The two innermost circles (almost on top of each other) circumvents the coagulated tissue region where the border has a temperature of 60°C and where there is a 99% probability of cell death ($\Omega = 4.6$), respectively. The outermost circle shows the border where there is a 63% probability of cell death ($\Omega = 1$).

The lesion size seen in figure 4.12 evaluated when using $\Omega = 4.6$ as presented in table 4.6 is about 15 mm in diameter and almost overlaps with the estimation of using 60°C as an indicator for tissue coagulation, while the lesion size becomes 23.8 mm if $\Omega = 1$ is used. Evaluating tissue damage using $\Omega = 4.6$ gives a lesion size close to the average of the experiments, only differing by +0.6 mm in width and +0.2 mm in height, whereas using $\Omega = 1$ leads to a large overestimation of the lesion size. Both using 60°C as a threshold temperature for tissue coagulation and $\Omega = 4.6$ seem to be good indicators of thermally induced damage on tissue *ex vivo*. The result from using $\Omega = 1$ to evaluate the lesion size gives a volume of irreversible damaged tissue which includes damage due to hyperthermic temperatures (about 42-50°C) which is relevant in *in vivo* settings, where a lesion size of about 20 mm in diameter is expected with this set-up [6].

TABLE 4.6: The results from the experiments that yielded the most average, minimum, and maximum of the parameter values measured. As well as the results from the simulations where recursive tissue coagulation was implemented. $D_{th,55°C}$ and $D_{th,60°C}$ represent the simulations where a threshold of 55°C and 60°C were used to recursively determine thermal coagulation respectively. $D_{th,60°C,\Omega=4.6}$ evaluates the lesion size using the Arrhenius equation for data belonging to the simulation regarding $D_{th,60°C}$.

Results from	t_{warmup} [s]	d_{lesion} [mm]	E_{tot} [J]
$D_{th,55°C}$ (simulation)	100	17.1	2634
$D_{th,60°C}$ (simulation)	98	14.6	2524
$D_{th,60°C,\Omega=4.6}$ (simulation)	98	15.0	2524
Average (experiments)	95.6	14.4×14.8	2875
Minimum (experiments)	42	9×9	1960
Maximum (experiments)	158	19×20	4124

An *in vivo* imILT study on porcine skeletal muscle tissue using a similiar set-up as in this thesis, but with the master probe positioned at 15 mm away from the optical fiber, resulted in a measured lesion size of 34±9 mm in width and 30±7 mm in height, yielding an average diameter of approximately 30 mm [5]. Following the expectations of the total accumulated lesion for the imILT treatment if the master probe would be positioned 10 mm from the optical fiber, the average diameter of the lesion size would be approximately 20 mm, i.e a size two times bigger than the light source to master probe distance. The theoretical calculated lesion size

in the model using $\Omega = 1$ as per figure 4.12 yielded a lesion size of 3.8 mm larger than the *in vivo* study results in [5]. Note however, that in this case, the model incorporates parameters for bovine cardiac muscle tissue, and not porcine skeletal muscle tissue, so the arrhenius parameters and the optical and thermal parameters in the model are inaccurate in the comparison. Also that the model does not take effects such as blood perfusion into consideration. The model however, gives a reasonable lesion size in this crude comparison to the *in vivo* measurements in [5]. The theoretical model evaluating tissue damage using the Arrhenius approach might thus be useful for both *ex vivo* and *in vivo* treatment planning.

There are however sources of error accompanying the simulation models developed in this thesis. The method used to modulate the thermal properties is erroneous for temperatures above 100°C as this is the boiling point of water and the description therefore becomes much less accurate. As figure 4.11 (d) shows temperatures well above 100°C were achieved in the simulations. Furthermore, when water residing in tissue boils some of the energy that contributes to temperature increase is used to change water from liquid to gas phase. The temperature rise in tissue would therefore be delayed at times when water boils. As tissue boils and steam bubbles form and possibly coalesce leaving holes in the tissue, the complexity of the model significantly increases. When it comes to the recursive modulation of the optical properties the used temperature thresholds for thermal coagulation are implemented under the assumption that at tissue regions where this temperature is achieved thermal coagulation occurs instantly. This is however not the case seen in experiments from previous studies, where a temperature of 60°C only lead to irreversible damage after about 6 s of exposure while 55°C lead to irreversible damage first after about 50 s [18]. This implies that the border separating thermally coagulated tissue and undamaged tissue might have been overestimated, especially for the case where 55°C was used. Considering the evaluation of thermal damage using the Arrhenius approach an uncertainty especially lies with the two parameters A (frequency factor) and ΔE_a (activation energy) since experimental data for these parameters are difficult to obtain. This is due to the inhomogeneity of tissues as well the difficulty of choosing an appropriate physical marker to asses thermal damage. Despite these errors the results from this simulation study are in good qualitative agreement with the experimental results, which is shown in table 4.6.

Chapter 5

Conclusions & Outlook

Both an experimental and theoretical study of immunostimulating interstitial laser thermotherapy on bovine cardiac muscle tissue was performed to evaluate how well a theoretical model can predict the outcome an *ex vivo* imILT treatment. The theoretical study was also performed to evaluate the significance of variations in thermal and optical properties of tissue, such as absorption, scattering, and thermal conductivity. It was furthermore used to investigate the effect of dynamic tissue properties on the treatment results. This by the implementation of fixed and recursive coagulation volumes.

From the simulation results it is seen that an increase in the absorption coefficient implies that the light is absorbed within a smaller volume. This results in a faster temperature rise close to the light source while the temperature rise of tissue further away is slower. An increase in the scattering coefficient yields a similar effect. Increasing the heat conductivity of tissue increases the rate of heat transport throughout the tissue decreasing the maximum temperature achieved close to the light source. A similar behaviour is observed if the amount of coagulated tissue around the fiber is increased. Modelling recursive coagulation of tissue using a threshold temperature yields similar effects as implementing coagulation zones close to the light source. From the simulations it was concluded that a change in all of the optical properties affects the result in the same way; therefore it is difficult to identify the individual contributions. It was found that the heat conductivity is the most important thermal property of tissue. Its large uncertainty and the large impact it yields makes it more relevant to calculate the heat conductivity dynamically based on tissue water content, as done in the last

simulation study presented in this thesis.

The results of the simulated imILT treatment of bovine cardiac muscle generated by the model developed in this thesis are in overall agreement with the experimental results. It is the implementation of recursive changes on the optical and thermal properties that seems to give the best agreement with the experiments. The simulation where a temperature threshold of 60°C was implemented to determine thermal coagulation, generated the results that were closer to the average of the results of the experiments. A similar lesion size was obtained when evaluating the damaged volume using the Arrhenius equation, where $\Omega = 4.6$ was considered the threshold value to define the damaged tissue (99% cell death). $\Omega = 1$ (63% cell death) yielded a lesion size that is compatible with expected *in vivo* results.

For future usability of the model more experiments are needed to validate it. This since the experimental results varied noticeably between the treatments, and therefore implies that the average of the results from the experiments performed might be either over or underestimated. The diffusion approximation of light transport might not be good enough to simulate the light distribution and a more accurate description of light transport, such as using Monte Carlo based on the radiative transfer theory, might be needed. The assumption of using a point source to replace a physical optical fiber might be erroneous and could be improved by implementing the irradiation profile from the fiber of interest. The heat conductivity needs to be evaluated more precisely for the tissue treated, possibly based on water content. Improved measurements of the optical properties for the tissue of interest are needed due to their large impact on the treatment, especially at stages where tissue coagulates. Furthermore, only using a two-step change in the optical properties dependent on a temperature threshold for thermal coagulation might be inaccurate and a more dynamic approach is needed, such as the Arrhenius approach which also depends on time of heat exposure. The Arrhenius parameters are however difficult to measure. Despite these possible restrictions to the model developed in this thesis it can be made useful for predicting treatment outcomes for different tissue types *ex vivo*, and can be used to for example assess the necessary input power needed to treat a specific region in the tissue of interest, or where to place the master probe. It is also promising for the more complicated *in vivo* treatments where it can be potentially used during treatment planning to determine the treatment dosimetry to, for example avoid unnecessary damage

to healthy tissue and carbonization. In *in vivo* settings the model however needs to include parameters such as blood perfusion, and effects due to local inhomogeneities such as for example blood vessels. The model can be further expanded to for example include a defined region of tumorous tissue surrounded by healthy tissue to further mimic reality.

Bibliography

[1] S.G. Bown. *Phototherapy of Tumors*. World J. Surg. 7:700-709, 1983.

[2] D.F. Saldanha, V.L. Khiatani, T.C. Carrillo, F.Y. Yap, J.T. Bui, M.G. Knuttinen, C.A. Owens and R.C. Gaba. *Current Tumor Ablation Technologies: Basic Science and Device Review*. Seminars in interventional Radiology 27(3):247-54, 2010.

[3] C. Sturesson. *Medical Laser-Induced Thermotherapy - Models and Applications*. Ph.D. thesis, Lund University, 1998.

[4] Clinical Laserthermia Systems AB. imILT$^{\text{CLS}}$
URL: www.imilt.se [Accessed on January 9, 2017].

[5] C. Pantaleone, S. Dymling, and J. Axelsson. *Optical fiber solutions for laser ablation of tissue and immunostimulating interstitial laser thermotherapy - product development in the network of developers, industry and users*. Photon Lasers Med 2015;aop, pages 2 and 3, 2015.

[6] P.H. Möller, K. Ivarsson, U. Stenram, M. Radnell, K.G. Tranberg. *Interstitial laser thermotherapy of adenocarcinoma transplanted into rat liver*. Eur J Surg 163(11):861-70, 1997.

[7] K. Ivarsson, L. Myllymäki, K. Jansner, U. Stenram, K.G. Tranberg. *Resistance to tumour challenge after tumour laser thermotherapy is associated with a cellular immune response*. Br J Cancer 93(4):435-40, 2005.

[8] I.A. Chang. *Considerations for Thermal Injury Analysis for RF Ablation Devices*. Open Biomed Eng J Vol. 4,p. 3-12, February 2010.

[9] E. Emilsson. *Source model for Immunostimulating Interstitial Laser Thermotherapy dosimetry*. Master thesis, Lund University, 2017.

[10] S. Svanberg. *Atomic and molecular spectroscopy*. Springer, 2001.

[11] T. Svensson. *Pharmaceutical and Biomedical Applications of Spectroscopy in the Photon Migration Regime*. Ph.D. thesis, Lund university, 2008.

[12] C.F. Bohren, D.R. Huffman. *Absorption and Scattering of Light by Small Particles*. John Wiley & Sons Inc., 1983.

[13] Ishimaru. *Wave Propagation and Scattering in Random Media*. Academic, New York, VOL. 1, Chap. 7, p. 147, 1978.

[14] A.J. Welch, M.J.C. van Gemert (Eds.). *Optical-Thermal Response of Laser-Irradiated Tissue 2nd ed.*. Springer Netherlands, 2011.

[15] J.A. Parrish. *New concepts in therapeutic photomedicine: photochemistry, optical targeting and the therapeutic window*. J. Invest. Dermatol. 77(1):45–50, 1981.

[16] L.V. Wang, H. Wu. *Biomedical Optics - Principles and Imaging*. Wiley & Sons, Inc., Hoboken, New Jersey, Chap. 1, p. 2, 2007.

[17] S.L. Jacques, B.W Pogue. *Tutorial on Diffuse Light Transport*. J. of Biomedical Optics 13(4), 041302, 2008.

[18] M.H. Niemz. *Laser–Tissue Interactions* Springer-Verlag, 3rd edition, 2007.

[19] COMSOL. *Heat Transfer Module User's Guide*. Version 5.2, 2015.

[20] J. Heisterkamp, R. van Hillegersberg, J.N.M IJzermans. *Critical temperature and heating time for coagulation damage: implications for interstitial laser coagulation (ILC) of tumors*. Lasers Surg. Med. 25(3):257-262, 1999.

[21] H.M. Sweetland, A. Wyman. K. Rogers. *Evaluation of the effect on normal liver of interstitial laser hyperthermia using artificial sapphire probes*. Lasers Med. Sci. 8: 99-105, 1993.

[22] S. Thomsen. *Identification of lethal thermal injury at the time of photothermal treatment*. Pages 459-467 in: G.J. Müller, A. Roggan. *Laser-Induced Interstitial Thermotherapy*. SPIE - The International Society for Optical Engineering, Bellingham, Washington, USA, 1995.

[23] G.L. LeCarpentier, M. Motamedi, L.P. McMath, S. Rastegar. A.J. Welch. *Continuous wave laser ablation of tissue: analysis of thermal and mechanical events*. IEEE Trans. Biomed. Eng. 40(2):188-200, February 1993.

[24] D.B. Leper. *Molecular and cellular mechanisms of hyperthermia alone or combined with other modalities*. Pages 9-40 in: J. Overgaard (ed.). *Hyperthermic Oncology*. Taylor and Francis, London, vol. 2, 1984.

[25] C. Streffer. *Mechanism of heat injury*. Pages 213-222 in: J. Overgaard (ed.). *Hyperthermic Oncology*. Taylor and Francis, London, 1984.

[26] G.M. Hahn. *Hyperthermia and cancer*. Plenum, New York, 1982.

[27] J.E. Fuhr. *Effect of hyperthermia on protein biosynthesis in L5178Y murine leukemic lymphoblasts*. J Cell. Physiol. 84(3):365-371, 1974.

[28] J.L. Roti Roti and A. Laszlo. *The effects of hyperthermia on cellular macromolecules*. pages 13-56 in: M. Urano, E. Douple (eds.). *Hyperthermia and oncology*. VSP, Utrecht, Netherlands, vol. 1, 1988.

[29] B.V. Harmon, Y.S. Takano, C.M. Winterford, G.C. Gobé. *The role of apoptosis in the response of cells and tumours to mild hyperthermia*. Int. J. Radiat. Biol. 59(2):489-501, February 1991.

[30] S. Thomsen. *Pathologic analysis of photothermal and photomechanical effects of laser-tissue interactions*. Photochem. Photobiol. 53(6):825-835, June 1991.

[31] M. Nikfarjam, V. Muralidharan, C. Christophi: *Mechanisms of Focal Heat Destruction of Liver Tumors*. J. Surg. Res. Vol. 127, issue 2, p. 208-223, August 2005.

[32] K. F. Chu, D. E. Dupuy. *Thermal ablation of tumours: biological mechanisms and advances in therapy*. Nature Reviews Cancer Vol. 14. p. 199-208, February 2014.

[33] COMSOL. COMSOL Multiphysics®
URL: www.comsol.se/comsol-multiphysics [Accessed on February 3, 2017].

[34] I.A. Chang, U.D. Nguyen. *Thermal modeling of lesion growth with radiofrequency ablation devices*. Biomed Eng Online, 3(27), Aug 2004.

[35] A. Roggan, G.J. Müller. *Dosimetry and computer based irradiation planning for laser-induced interstitial thermotherapy (LITT)*. Pages 114–157 in: G.J. Müller, A. Roggan. *Laser-Induced Interstitial Thermotherapy*. SPIE - The International Society for Optical Engineering, Bellingham, Washington, USA, 1995.

[36] G.J. Müller, A. Roggan. *Laser-Induced Interstitial Thermotherapy*. SPIE - The International Society for Optical Engineering, Bellingham, Washington, USA, 1995.

[37] N. Akashi, J. Kushibiki, N. Chubachi, F. Dunn. *Acoustic properties of selected bovine tissues in the frequency range 20-200 MHz*. The Journal of the Acoustical Society of America 98(6), 1995.

[38] F.A. Duck. *Physical Properties of Tissues: A Comprehensive Reference book*. Academic Press, Sand Diego, CA, USA, 1990.

[39] JC Chato (ed.). *Thermal Problems in Biotechnology*. ASME symposium series, American Society of Mechanical Engineers, New York, 1968.

[40] H.F. Bowman, E.G. Cravalho, M. Woods. *Theory, Measurement, and Application of Thermal Properties of Biomaterials*. Annual Review of Biophysics and Bioengineering Vol. 4:1-577, June 1975.

[41] R. Agah, A.H. Gandjbakhche, M. Motamedi, R. Nossal, R.F. Bonner. *Dynamics of Temperature Dependent Optical Properties of Tissue: Dependence on Thermally Induced Alteration*. IEEE Transactions on Biomedical Engineering 43(8):839-846, August 1996.

[42] V. Rajanayagam, M.E. Fabry, J.C Gore. *In vivo quantitation of water content in muscle tissues by NMR imaging*. Magnetic Resonance Imaging 9(4):621-625, January 1991.